The export of African mineral dust across the Atlantic and its impact over the Amazon Basin

Xurong Wang[1,2,a,+], Qiaoqiao Wang[1,2,+], Maria Prass[3], Christopher Pöhlker[3], Daniel Moran-Zuloaga[3], Paulo Artaxo[4] Jianwei Gu[5], Ning Yang[1,2], Xiajie Yang[1,2], Jiangchuan Tao[1,2], Juan Hong[1,2], Nan Ma[1,2], Yafang Cheng[3], Hang Su[3], Meinrat O. Andreae[3,6]

[1.] Institute for Environmental and Climate Research, Jinan University, Guangzhou, 511443, China

[2.] Guangdong-Hongkong-Macau Joint Laboratory of Collaborative Innovation for Environmental Quality, Guangzhou, 511443, China

[3.] Multiphase Chemistry Department, Max Planck Institute for Chemistry, Mainz, 55128, Germany

[4.] Institute of Physics, University of São Paulo, São Paulo, 05508-900, Brazil

[5.] Institute of Environmental Health and Pollution Control, School of Environmental Science and Engineering, Guangdong University of Technology, Guangzhou, 510006, China

[6.] Scripps Institution of Oceanography, University of California, San Diego, CA 92093-0230, USA

[a.] now at: Institute of Energy and Climate Research, IEK-8, Forschungszentrum Jülich, Jülich, 52428, Germany

[+.] These authors contribute equally to this article

Correspondence to, Qiaoqiao Wang (qwang@jnu.edu.cn)

Abstract

The Amazon Basin is frequently influenced by the trans-Atlantic transport of African dust plumes during its wet season (January – April), which not only interrupts the near-pristine atmospheric condition in that season, but also provides nutrient inputs into the Amazon rainforest upon deposition. In this study, we use the chemical transport model GEOS-Chem to investigate the impact of the export of African mineral dust to the Amazon Basin during the period of 2013 – 2017, constrained by multiple datasets obtained from AERONET, MODIS, as well as Cayenne site and the Amazon Tall Tower Observatory (ATTO) site in the Amazon Basin. With an optimized particle mass size distribution (PMSD) of dust aerosols, the model well captures observed AOD regarding both the mean value as well as the decline rate of the logarithm of AOD over the Atlantic Ocean along the transport path (AOaTP), implying the consistence with observed export efficiency of African dust along the trans-Atlantic transport. With an annual emission of 0.73 ± 0.12 Pg yr^{-1}, African dust entering the Amazon Basin during the wet season accounts for 40% ± 4.5% (up to

70%) of surface aerosol mass concentrations over the basin. Observed dust peaks over the Amazon Basin are generally associated with relatively higher African dust emissions (including Sahara and Sahel) and longer lifetime of dust along the trans-Atlantic transport, namely higher export efficiency of African dust across the Atlantic Ocean. The frequency of dust events during the wet season is around 18% averaged over the Amazon Basin, with maxima over 60% at the northeast coast. During the dust events, AOD over most of the Amazon Basin is dominated by dust. Based on dust deposition, we further estimate annual inputs of 52 ± 8.7, 0.97 ± 0.16 and 21 ± 3.6 mg m^{-2} yr^{-1} for iron, phosphorus and magnesium, respectively, into the Amazon rainforest, which may to some extent compensate the hydrologic losses of nutrients in the forest ecosystem.

1   Introduction

The desert in northern Africa, being the world's largest dust source, contributes to over 50% of global dust emission (Kok et al., 2021; Wang et al., 2016). Dust particles are uplifted by strong surface winds, and then typically transported downwind for a long distance, reaching Atlantic, Caribbean, America, and Europe (Prospero et al., 1981; Ben-Ami et al., 2012; Yu et al., 2019; Swap et al., 1992; Prospero et al., 2014; Wang et al., 2020). The emission varies on daily to seasonal and even decadal time scales, largely affected by local wind speed, land surface cover, soil moisture, etc (Ridley et al., 2014; Mahowald et al., 2006). Once present in the atmosphere, mineral dust can not only degrade air quality downwind, but also affect the radiation balance of the Earth-Atmosphere system directly by scattering or absorbing solar radiation (Ryder et al., 2013b), and indirectly by altering cloud properties via acting as cloud condensation nuclei or ice nuclei (Chen et al., 1998; Demott et al., 2003; Mahowald and Kiehl, 2003; Dusek et al., 2006). Additionally, mineral dust contains iron, phosphorous, and other nutrients, and could affect ocean biogeochemistry and fertilize tropical forest upon downwind deposition (Niedermeier et al., 2014; Rizzolo et al., 2017).

64   There is an increased concern about the impact of African dust exerted over the

65   Amazon basin, which being the world's largest rainforest, represents a valuable but

66   also vulnerable ecosystem, and is sensitive to any disturbance from climate changes

67   associated with human activities in the future (Andreae et al., 2015; Pöhlker et al.,

68   2019). During the wet season (January – April) Amazonian aerosols are generally

69   dominated by local biogenic aerosols, with remarkably low PM_{10} mass concentrations

70   of a few $\mu g\ m^{-3}$ (Andreae et al., 2015; Martin et al., 2010a; Prass et al., 2021). The

71   near-pristine condition, however, is frequently interrupted by the transatlantic

72   transport of African dust toward the Amazon Basin (Andreae et al., 2015; Martin et

73   al., 2010b; Martin et al., 2010a; Talbot et al., 1990). The dusty episodes could

74   drastically increase aerosol optical depth (AOD, by a factor of 4), mass concentrations

75   of coarse aerosols (with diameter > 1 μm, up to 100 $\mu g\ m^{-3}$), as well as crustal

76   elements over the Amazon Basin (Ben-Ami et al., 2010; Pöhlker et al., 2019; Moran-

77   Zuloaga et al., 2018; Baars et al., 2011; Formenti et al., 2001). Therefore, there is

78   great interest in understanding factors controlling the export of African dust towards

79   the Amazon Basin and the impact they might have on environment, ecosystem, and

80   climate.

81   Over the past decades, field measurements combined with satellite observation and

82   forward/back trajectory analysis have been conducted to explore the long-range

83   transport (LRT) of African dust toward the Amazon Basin (e.g. Ben-Ami et al., 2010;

84   Pöhlker et al., 2018; Prospero et al., 2020). The transatlantic transport of African dust

85   plumes is closely related to annual north-south oscillation of the intertropical

86   convergence zone (ITCZ) (Moran-Zuloaga et al., 2018; Ben-Ami et al., 2012),

87   favoring the path towards the Amazon Basin in the late boreal winter and spring

88   (December-April) as the ITCZ moves southward. In addition to the annual oscillation

89   of ITCZ, the export efficiency of African dust towards the Amazon Basin also highly

90   depends on the atmospheric lifetime of mineral dust, which is largely affected by

91   meteorological conditions (e.g. precipitation). Dust particles are subject to wet

92   removal when they are within or underneath precipitating clouds. For instance, Yu et

al. (2020) argued that El Djouf, in western Sahara, contributes more dust to the Amazon Basin than the Bodélé depression as the transport paths of dust released from El Djouf are less affected by rainy clouds.

Besides meteorological conditions, the lifetime of dust particles and consequently the export efficiency of African dust towards the Amazon Basin could also be affected by the size distribution of dust particles. Previous studies have observed that volume/mass fractions of coarse mode dust particles, giant particles in particular, tend to be reduced along the transport due to their higher gravitational settling velocities (Ryder et al., 2018; Ryder et al., 2013b; Ryder et al., 2013a; Van Der Does et al., 2016). Moreover, the optical properties of mineral dust are also strongly size dependent, especially for those in sub-micron range (Liu et al., 2018; Di Biagio et al., 2019; Ysard et al., 2018). For instance, Ryder et al. (2013a) reported a loss of $60 - 90\%$ of particles with diameter > 30 μm 12 h after uplift and consequently an increase in the single scattering albedo from 0.92 to 0.95 associated with the change in the size distribution of dust aerosols. Therefore, the size distribution of dust particles is a key factor determining the efficiency of dust transport and consequently the environmental and climate effect of the mineral dust downwind (Mahowald et al., 2011a; Mahowald et al., 2011b).

So far, a few studies have attempted to quantify the impact of the LRT of African dust over the Amazon Basin, but mainly focus on dust deposition only (e.g. Yu et al., 2015a; Ridley et al., 2012; Yu et al., 2019). The estimates of annual dust deposition and deposition rates into the Amazon Basin exhibit a wide range (7.7-50 Tg yr^{-1} and 0.8-19 g m^{-2} yr^{-1}, respectively), attributed to the application of different methods and the intrinsic uncertainties associated with each method (Kok et al., 2021; Yu et al., 2015b; Kaufman, 2005; Swap et al., 1992). For example, the results based on Cloud-Aerosol Lidar and Infrared Pathfinder Satellite Observations (CALIPSO) is subject to the uncertainty associated with the Cloud-Aerosol Lidar with Orthogonal Polarization (CALIOP) extinction, vertical profile shape, dust discrimination, diurnal variations of dust transport as well as the below-cloud dust missed by CALIOP (Yu et al., 2015a).

While models could be considered as a useful tool to comprehensively assess the transatlantic transport of African dust towards the Amazon Basin and the consequent impact over the Amazon Basin, there exist considerable differences among model results, attributed to the uncertainties associated with the dust parameterization in the model, including emission schemes, size distributions of dust particles, dust deposition, etc (Kim et al.,2014; Huneeus et al., 2011; Mahowald et al., 2014). Observational constraints on the modelling results along the transport from source regions to receptor regions are thus in urgent need to accomplish a better evaluation of factors controlling the LRT of African dust and its overall impact over the Amazon Basin.

Here, we present a detailed multiyear simulation of the export of African dust across the Atlantic and its impact over the Amazon Basin (around $8.8 \times 10^6 \ km^2$, see Figure 1 for the defined area) during $2013 - 2017$ with the chemical transport model GEOS-Chem. The aims of this study are: (1) to evaluate the model performance of dust simulation including the particle mass size distribution (PMSD), optical properties, mass concentrations as well as the export efficiency of African dust towards the Amazon Basin; (2) to analyze factors controlling the export of African dust towards the Amazon Basin; and (3) to give a comprehensive examination of the impact of African dust over the Amazon Basin, including surface aerosol concentrations, AOD and nutrient inputs upon deposition. The paper is organized as follows: Section 2 describes the model setup for dust simulation and the observational datasets applied to constrain the model results; Section 3 gives the model evaluation regarding the simulation of the export of African dust towards the Amazon Basin; Section 4 presents the model results, including simulated dust emissions in Africa, the trans-Atlantic transport of African dust, and the influence of African dust over the Amazon Basin; and Section 5 summarizes the main conclusions drawn from this study.

2   Methodology

2.1 GEOS-Chem model

2.1.1 Model overview

In this study we use the GEOS-Chem model version 12.0.0 (www. geos-chem.org) to perform the global aerosol simulation with a horizontal resolution of 2° × 2.5º. The GEOS-Chem is driven by assimilated meteorological data GEOS-FP from the NASA Global Modeling and Assimilation Office (GMAO) (Lucchesi, 2013) with a native horizontal resolution of 0.25° × 0.3125°, which is then degraded to 2° × 2.5° for the input to GEOS-Chem. We initialize the model with a 1-year spin-up followed by an aerosol simulation from 2013 to 2017.

The aerosol simulation is an offline simulation for aerosol tracers including black carbon (BC), organic aerosols (OA), sulfate-nitrate-ammonium aerosols in fine mode ($\leqslant$ 1 μm in diameter), sea salt in both fine and coarse (> 1 μm in diameter) modes, and mineral dust in four size bins covering the size range of 0.2 – 12 μm in diameter. Aerosol optical properties used for aerosol optical depth (AOD) calculation are mainly based on Global Aerosol Data Set (Koepke et al., 1997), with modifications in aerosol size distributions (Jaeglé et al., 2011; Drury et al., 2010; Wang et al., 2003a; Wang et al., 2003b), hygroscopic growth factors of organic aerosols (Jimenez et al., 2009), and the refractive index of dust (Sinyuk et al., 2003). AOD in the model is then calculated online at selected wavelengths assuming lognormal size distributions of externally mixed aerosols and accounts for hygroscopic growth (Martin et al., 2003). Wet deposition in GEOS-Chem, based on the scheme of Liu et al. (2001), accounts for scavenging in both convective updrafts and large-scale precipitation. Further updates by Wang et al. (2011) are also applied, accounting for ice/snow scavenging as well as the impaction scavenging in convective updrafts. Dry deposition in the model follows the standard resistance-in-series scheme by Wesely (2007), accounting for turbulent transfer and gravitational settling (Wang et al., 1998; Zhang et al., 2001).

2.1.2 Dust emission and PMSD schemes in the model

The emission of mineral dust is based on the dust entrainment and deposition (DEAD) mobilization scheme of Zender et al. (2003) in the GEOS-Chem model. The DEAD scheme calculates the total vertical dust flux based on the total horizontal saltation

flux (Q_s) using the theory of White (1979). The Q_s depends mainly on the surface

wind friction velocity and the threshold friction velocity, which is determined by soil

type, soil moisture content, and surface roughness. For more details of the DEAD

scheme, readers are referred to Duncan Fairlie et al. (2007).

Freshly emitted dust particles are divided into four size bins in GEOS-Chem: $0.1 -$

1.0 μm, $1.0 - 1.8$ μm, $1.8 - 3.0$ μm, and $3.0 - 6.0$ μm in radius. The first size bin is

further divided into four sub-bins ($0.1 - 0.18$ μm, $0.18 - 0.3$ μm, $0.3 - 0.6$ μm, and

$0.6 - 1.0$ μm in radius) for the calculation of optical properties. While total dust

emissions are not affected, optical properties, atmospheric lifetime, and downwind

concentrations of dust particles are sensitive to different PMSD schemes. Table 1

shows 3 different PMSD schemes tested in this study: V12, V12_C and V12_F.

Scheme V12, which is derived based on scale-invariant fragmentation theory (Kok,

2011) with modification in tunable parameters (Zhang et al., 2013), is a default set in

GEOS-Chem. However, this scheme has been only evaluated for US/Asian dust, not

for Africa. On the other hand, V12_C was used in older versions of GEOS-Chem and

constrained from aircraft measurements during the Saharan Dust Experiment (Ridley

et al., 2012; Highwood et al., 2003). In addition, we derived V12_F based on the

Fennec airborne observations, which also focuses on Saharan dust. Among all the

three PMSD, V12_C has the largest mass fraction in the first bin (relatively small

particles) and the lowest fraction in the last bin (large ones). In contrast, V12_F has

the most dust distributed in the last bin ($\sim 70\%$) and only a little (around 5%) in the

first bin ($0.1 - 1.0$ μm). Simulated mass extinction efficiency (MEE, also shown in

Table 1) at wavelength of 550 nm for dust particles in the first sub-bin ($0.1 - 0.18$ μm)

is 3.13 $m^2\ g^{-1}$ and decreases to 0.16 $m^2\ g^{-1}$ for those in the last bin ($3.0 - 6.0$ μm). The

lifetime of dust aerosols against deposition are 5.1, 2.2, 1.7 and 0.86 d in the four bins

(from small to large size), respectively. Therefore, although with the same emission,

total dust AOD, lifetime, and downwind concentrations could vary greatly with

PMSD upon emissions. In this study, we will evaluate these three PMSD schemes and

the impact on AOD, dust concentrations as well as its export efficiency along the

209   trans-Atlantic transport from Africa to the Amazon Basin.

210   **2.2 Observations**

211   The study uses observations from multiple datasets obtained from AERONET,

212   MODIS, as well as Cayenne site and the Amazon Tall Tower Observatory (ATTO) site

213   to constrain model results regarding the simulation of the dust export from Africa to

214   the Amazon Basin. Table 2 summarizes these observations, including the parameters,

215   the spatio-temporal coverage, and the corresponding application in the model. The

216   daily data of AOD (at wavelength of 675 nm) and particle volume size distribution

217   (PVSD) from AERONET level 2.0

218   (aeronet.gsfc.nasa.gov/new_web/download_all_v3_ aod.html, last access on Jun. 22,

219   2021(Dubovik et al., 2002)) during the year of $2013 - 2017$ is used in the study to

220   evaluate dust emissions and its PMSD over the source regions in Africa in the model.

221   The PVSD data provided by AERONET is a column-integrated aerosol volume size

222   distribution with a size range of $0.05 - 15.0$ μm. It is then converted to PMSD using

223   the same densities as in the model. Only sites with valid data accounting for more

224   than 30% of the total are considered in this study. In addition, to minimize the

225   influence of aerosols other than dust, only data dominated by dust (simulated dust

226   contribution to column-integrated aerosols mass concentrations > 95%) is used for the

227   comparison of PMSD. There are a few sites not far from the coast and could be

228   influenced by sea salt. With the above data screening, the sea salt contribution to total

229   aerosol mass is less than 0.5%. For the comparison of AOD, the criterion is less

230   stringent to have more data points available and uses data dominated by coarse

231   aerosols (the contribution of fine aerosol to total aerosol volume < 3%). This criterion

232   does not exclude sea salt and the contribution of sea salt to AOD could be up to 30%

233   at the Capo_Verde site (22.9° W,16.7° N, in the east-central Atlantic Ocean).

234   The study also uses observed PMSD over central Sahara during Fennec Campaign

235   (africanclimateoxford.net/projects/fennec/, last access: 22 June 2021) for the

236   comparison with AERONET and our model results. Aiming to investigate dust

237   microphysical and optical properties, 42 profiles of particle size distribution $(0.1 -$

300 µm in diameter) over both the Sahara and the Atlantic Ocean were sampled from in-situ aircraft measurements during Fennec campaign. For more detailed description of the aircraft measurements, readers are referred to Ryder et al. (2013a).

In addition to AERONET AOD data, level 3 daily AOD (at wavelength of 550 nm) data from the moderate resolution imaging spectroradiometers (MODIS) installed on Terra and Aqua platforms (https://ladsweb.modaps.eosdis.nasa.gov/archive/allData/61/, last access: 22 June 2021) is applied in the study to evaluate the trans-Atlantic transport of dust plumes from Africa toward the Amazon Basin. For comparison, we degraded the original horizontal resolution of MODIS data ($1° \times 1°$) to $2° \times 2.5°$, consistent with the model outputs.

Finally, daily PM_{10} mass concentrations during wet season (from January to April) in 2014 measured at Cayenne, French Guiana ($52.3097°$ W, $4.9489°$ N, located in the northeast coast of the Amazon Basin, https://doi.org/10.17604/vrsh-w974, marked in Figure 1) and long-term aerosol measurements at the Amazon Tall Tower Observatory, Brazil (ATTO, $59.0056°$ W, $2.1459°$ S, located in the central Amazon Basin, also marked in Figure 1) are used in this study to further evaluate the model performance regarding the influence of the LRT of African dust over the Amazon Basin. The measurement at Cayenne site is carried out on a cooperative basis by personnel of ATMO-Guyane, a non-profit organization. The PM_{10} samples are measured by a Taper Element Oscillating Microbalance (TEOM, model 1400 series, ThermoFisher Scientific) and then are returned to Miami for analysis (Prospero et al., 2020). Readers are referred to Prospero et al. (2020) for detailed description of the site and the data. The ATTO site was established in 2012 for the long-term monitoring of climatic, biogeochemical, and atmospheric conditions in the Amazon rainforest. Detailed description of the site and the measurements there could be found in Andreae et al. (2015). In this study, we only use the particle number size distribution from an Optical Particle Sizer (OPS, TSI model 3330; size range of $0.3 - 10$ µm in diameter, divided into 16 size bins) and a Scanning Mobility Particle Sizer (SMPS, TSI model

3080, St. Paul, MU, USA; size range of 10 – 430 nm in diameter, divided into 104

size bins) over the period from 2014 to 2016. The number size distribution is

converted to mass concentrations assuming spherical particles with a constant density

of 1.5 g cm^{-3} (Pöschl et al., 2010).

3 Model evaluation

Here we evaluate three different PMSD schemes regarding the model performance of

dust simulation through the comparison with observed mass size distribution of

column-integrated aerosol over Africa, AOD over both Africa and the Atlantic Ocean,

as well as PM$_{10}$ and dust concentrations in the Amazon Basin. Figure 2 shows the

mass fractions of column-integrated aerosols retrieved from AERONET sites

compared with model results based on different PMSD schemes. The location of the

selected AERONET sites with valid data are marked in Figure 1 as purple symbols

(including asterisks and circles). The mean mass fractions for each bin from

AERONET data are 17%, 27%, 38%,17%, respectively. The comparison indicates the

model results based on V12_C agrees better with the observations, with much smaller

mean absolute deviation (MAD) of 2.8, followed by 4.2 for V12 and 18 for V12_F. In

other words, the model results with other PMSD schemes (V12_F in particular)

greatly underestimate the mass fractions in the first bin and overestimate the mass

fractions in the last bin. During the Fennec campaign, the aircraft sampled two strong

Saharan dust outbreaks with AOD up to 1.1, which may be associated with strong

winds favoring the uplift of large particles.

Figure 3 shows the times series of daily AOD at wavelength of 675 nm during the

year of 2013 − 2017 from both AERONET and model results. The locations of the

selected AERONET sites with valid data over northern Africa are shown in Figure 1

as purple circles. The Capo_Verde site is also included to show the model

performance over the ocean in addition to the land. Although different PSD schemes

have little influence on the correlation between AERONET and model results with

most r around 0.6 − 0.7, the normalized mean bias (NMB) has been significantly

improved in V12_C, with a range of -12% − 11% (vs. -33% − -11% and -42% − -19% for V12 and V12_F, respectively). The severe underestimation in AOD from V12 and V12_F could be attributed to their relatively higher dust fractions distributed in larger size bins with relatively lower MEE.

In addition, we also compare the spatial distributions of simulated AOD over the Atlantic Ocean with MODIS AOD (at 550 nm) averaged over 2013 − 2017 in Figure 4a-d. There is a clear decreasing trend in MODIS AOD along the trans-Atlantic transport from Africa towards South America. Although all simulations show similar spatial distributions with declining trends of AOD along the transport, the results from V12_C are the most consistent with MODIS data with the highest r of 0.89 and the smallest NMB of 6.5% among the three schemes (vs. r of 0.85 and 0.81 and NMB of -13% and -19% for V12 and V12_F, respectively). Note that the model results based on V12_C tends to overestimate MODIS AOD over Africa while no significant systematic bias is found between V12_C and AERONET AOD. Wang et al. (2016) sampled MODIS data at AERONET sites over Africa and found that MODIS retrieval underestimated AERONET AOD at most sites with NMB of -12% − -36%, which partly explains the overestimates in MODIS AOD by V12_C here.

Assuming first-order removal of aerosol along the transport, we could derive the removal rates of aerosols, estimated as the gradient of the logarithm of AOD (log(AOD)) against the distance over the Atlantic Ocean along the transport path (AOaTP, 20° − 50° W and 5° S − 25° N, Figure 4e). The decline rate of MODIS log(AOD) is 0.019 ± 0.0025 degree^{-1}. A similar decline rate of 0.019 ± 0.0029 degree^{-1} is found for simulated log(AOD) based on V12_C. In contrast, simulations with V12 and V12_F exhibit relatively steeper slopes of 0.021 ± 0.0040 and 0.021 ± 0.0041, respectively, implying too much aerosol removal and thus lower export efficiency along the transport. To specify the impact of different PMSD on the export efficiency of dust aerosols towards the Amazon Basin, Figure 4f also shows simulated dust AOD (DOD) along the transect from 20° to 50° W. The DOD from V12_C decreases from 0.15 ± 0.018 to 0.049 ± 0.088 along the transport, with a decreasing rate of $0.016 \pm$

325   0.0014 degree^{-1}. In contrast, DOD decreases from 0.097 ± 0.012 to 0.028 ± 0.085 with

326   a slope of 0.018 ± 0.0016 for V12 and decreases from 0.080 ± 0.090 to 0.025 ± 0.084

327   with a slope of 0.017 ± 0.0014 for V12_F.

328   Lying in the trade wind belt, Cayenne has been taken as the gate of African dust.

329   Hence, the comparison between simulated and observed dust concentrations at

330   Cayenne site could help model evaluation in reproducing the arrival of African dust to

331   the Amazon Basin. As shown in Figure 5a, the simulation from V12_C shows

332   excellent agreement between simulated dust and observed PM_{10} concentrations during

333   the wet season, with r around 0.85 and NMB of -39%. The correlation from the other

334   two simulations is similar ($r = 0.86$), but the corresponding NMB is much larger (-

335   57% for V12 and -80% for V12_F). Based on the regression line between observed

336   concentrations of PM_{10} and dust at the same site, Prospero et al. (2020) obtained a

337   regional background value of PM_{10} ranging from 17 to 22 μg m^{-3}, largely attributed to

338   sea salt aerosols, and a value of 0.9 for the slope, suggesting PM_{10} values above this

339   range as a proxy for advected dust. Consistent with their results, the regression line

340   between simulated dust and PM_{10} from V12_C in this study shows a background

341   value of PM_{10} around 23 μg m^{-3}, with a value of the slope around 1.0, and the dust

342   contribution to PM_{10} is around 53% ± 20%. In contrast, the regression lines from V12

343   and V12_F are much steeper, with the slope of 1.4 and 2.1, respectively, and the dust

344   contributions are relatively smaller, 44% in V12 and 34% in V12_F.

345   We also compare simulated dust concentrations with observed coarse particles at the

346   ATTO site in central Amazon in the wet season during 2014 – 2016 in Figure 5b. The

347   correlation between observed and simulated data are similar for different PMSD

348   schemes with r of 0.63 − 0.65. But the bias of V12_C is negligible (NMB = -0.27%)

349   while both V12 and V12_F tend to underestimate the coarse aerosol concentrations

350   with NMB of -36% and -55%, respectively. The dust contribution to coarse aerosols is

351   above 80% in V12_C, but less than 70% in V12_F. This again implies relatively

352   higher export efficiency of African dust aerosols towards the Amazon Basin with

353   V12_C associated with their relatively higher dust fractions distributed in smaller size

354 bins.

355 Overall, compared with V12 and V12_F schemes, model results based on V12_C are

356 more consistent with the multiple observational datasets, including column-integrated

357 particle size distribution, AOD and surface coarse aerosol concentrations obtained

358 either over sources or downwind of the sources. Therefore, we use the model results

359 from V12_C (hereinafter referred to as model results unless noted otherwise) to

360 investigate the transatlantic transport of African dust and its impact over the Amazon

361 Basin in the following sections.

362

363 **4   Results and discussion**

364 **4.1 Dust emissions**

365 Figure 1 shows the spatial distribution of simulated dust emissions and Table 3 lists

366 seasonal and annual dust emissions in northern Africa ($17.5° \, W - 40° \, E$, $10° \, N - 35°$

367 N) for the period of $2013 - 2017$. Simulated annual dust emission from northern

368 Africa is 0.73 ± 0.12 Pg yr^{-1}, contributing more than 70% of the global dust emission

369 (0.99 ± 0.20 Pg yr^{-1}). The result is in the range of $0.42 - 2.05$ Pg yr^{-1} reported by Kim

370 et al. (2014), who evaluated five AeroCom II global models regarding the dust

371 simulation over similar regions.

372 There exists a strong seasonality in the dust emission from northern Africa, peaking in

373 spring and winter (up to 1.2 Pg yr^{-1}) and reaching the minimum in fall (around 0.33

374 Pg yr^{-1}) in general. Previous studies have also pointed out that dust emissions over

375 different African regions show distinct variations (Bakker et al., 2019; Shao et al.,

376 2010), attributed to differences in geographical properties (Knippertz et al., 2007),

377 vegetation cover (Mahowald et al., 2006; Kim et al., 2017), and meteorological

378 mechanisms on a local scale (Alizadeh-Choobari et al., 2014; Wang et al., 2017;

379 Roberts and Knippertz, 2012). Consequently, there exists substantial seasonal change

380 in different dust source regions. For instance, during boreal winter, the Bodélé

381 Depression in northern Chad is found to be the most active triggered by the Harmattan

382 winds, while the northwestern African dust sources become less active in contrast

383 with the condition in boreal summer (Ben-Ami et al., 2012; Prospero et al., 2014).

384 Therefore, we further analyze the emission variability over five different source

385 regions in northern Africa (Figure 1 and Table S1). On an annual basis, the

386 contribution to total northern African dust emission is the largest from Region A (west

387 Sahara, 36% ± 4.0%), followed by Region D (central Sahel including the Bodélé

388 Depression, 21% ± 4.7%), Region B (central Sahara, 13% ± 2.6%), Region C (east

389 Sahara, 12% ± 1.0%), and Region E (west Sahel, 6.5% ± 0.64%). The emission

390 fluxes, however, are the most intensive in Region D, up to 11 ± 2.1 g month^{-1} m^{-2} and

391 are generally below 5 g month^{-1} m^{-2} over the other regions.

392 Concerning the seasonality, higher dust emission tends to occur in boreal spring and

393 winter, with the largest emission flux of 19 ± 4.7 g month^{-1} m^{-2} from Region D. As

394 shown in Figure 6 and S1, the emissions peak in boreal spring for Region A, B and C,

395 but in winter for Region D and E. There is also a secondary peak in summer

396 emissions for Region E. Correlation analysis between dust emissions and

397 meteorological variables suggests that the seasonality is mainly driven by high surface

398 wind speeds (with r of 0.79-0.96 and 0.68-0.97 for the 75th and 95th percentiles of 10-

399 m wind speeds, respectively). Apparent negative correlation is also found between

400 precipitation (soil moisture, Figure S1) and dust emission in Region D with r of -0.69

401 (-0.67).

402 Similar seasonality is also reported by Cowie et al. (2014), who suggested that the

403 strongest dust season in winter in central Sahel is driven by strong harmattan winds

404 and frequent Low level Jet breakdown, and the second peak in summer in west Sahel

405 could be explained by the summer monsoon combined with the Sahara Heat Low. The

406 study also suggested the dominance of strong wind frequency in the seasonal variation

407 of the emission frequencies. Fiedler et al. (2013) also found a maximum of emission

408 flux over the Bodélé Depression in winter and the highest emission flux in spring in

409 west Sahara. The study suggested that near-surface peak winds associated with

410 Nocturnal Low-Level Jets serve as a driver of mineral dust emissions. Negative

411 correlation between dust emissions and soil moisture has also been revealed by Yu et

al. (2017) and Pierre et al. (2012), as the decreased vegetation growth in response to dry soil would result in enhanced dust emissions.

It is also worth noting that the interannual variation in dust emissions is much larger during the wet season (0.96 ± 0.25 Pg yr^{-1}, Table 3) than on an annual basis (0.73 ± 0.12 Pg yr^{-1}). Moreover, while the annual emissions gradually decrease from 2013 to 2017, the emissions during the wet season peak in 2015. The obviously different behavior between the annual emissions and emissions during the wet season suggests that predictions of the future impact of African dust emissions over the Amazon Basin in response to climate change should focus on the wet season rather than the annual average, as the former is more related to the export of African dust towards the Amazon Basin.

4.2 Transatlantic transport of African dust

The amount of African dust reaching the Amazon Basin depends not only on the dust emission fluxes, but also the transport paths. Associated with the annual oscillation of ITCZ, the outflow of African dust moves slightly southwest toward South America in boreal winter and spring, and moves west towards the Caribbean in boreal summer and fall (Moran-Zuloaga et al., 2018; Ben-Ami et al., 2012). The GEOS-Chem results in this study are consistent with this seasonal oscillation: although higher dust load over the coastal region of North Africa is found in boreal summer (> 500 mg m^{-2}), dust reaching the Amazon Basin is less than 10 mg m^{-2}; In contrast, dust load over the Amazon Basin could reach up to 50 mg m^{-2} in boreal spring and winter.

In addition to the transport paths, the amount of African dust arrival at the Amazon Basin is also sensitive to its removal rate, namely the lifetime against deposition over the Atlantic. Assuming first-order removal of dust aerosols, we further derived seasonal e-folding lifetime (hereinafter referred to as lifetime, τ) of simulated dust during $2013 - 2017$, based on the logarithm of the dust column burden against travel time over the AOaTP (Figure 7) using Equation 1:

$$\tau = \frac{L}{v \times slope} \qquad (1)$$

where L is the distance of 1-degree longitude averaged over $5° \text{ S} - 25° \text{ N}$ in unit of m degree^{-1}; v is the wind speed in unit of m s^{-1}; and $slope$ is the gradient of the linear

442 trend line based on the logarithm of dust burden against the distance in degree

443 between 20 ºW and 50 ºW.

444 Estimated dust lifetime is the shortest (1.4 $\pm$ 0.098 d) in winter, followed by fall and

445 spring (1.9 $\pm$ 0.33 d and 2.3 $\pm$ 0.31 d, respectively), while the lifetime in summer is

446 the longest (4.2 $\pm$ 0.68 d). The interannual variability of the lifetime is small in winter

447 with relative standard deviation (RSD) of 7.0%, but relatively large in fall with RSD

448 of 17%. The short lifetime in winter is generally associated with high deposition flux

449 (including both dry and wet deposition). As shown in Figure 8, the largest dust

450 deposition flux (> 1000 ng m^{-2} s^{-1}) is found over the source regions in northern Africa,

451 especially in spring and winter, and is mainly due to dry deposition (accounting for

452 more than 80%). As a result, 48% – 64% of total emission in northern Africa is

453 deposited within the source region (Table S2). The deposition flux over the AOaTP,

454 also shows strong seasonality, with a maximum of ~530 ng m^{-2} s^{-1} in winter and a

455 minimum of ~180 ng m^{-2} s^{-1} in fall, and is mainly driven by wet deposition

456 (accounting for 76% on average). The deposition over the AOaTP accounts for 20%

457 of total emission in northern Africa in winter, in contrast to 7.7% in spring, consistent

458 with the relatively shorter lifetime in winter discussed above.

459 The seasonality in the deposition fluxes and the consequent dust lifetime depends not

460 only on precipitation but also the vertical pathways of dust transport across the

461 Atlantic. Dust aerosols aloft at higher altitude reach further west and have relatively

462 longer lifetime. Significant differences in dust vertical distributions along the

463 transport pathways have been revealed from the CALIOP measurements, which show

464 that more dust is transported above 2km in summer while the dust layer is the

465 shallowest in winter (Liu et al., 2012).

466 **4.3 The influence of African dust over the Amazon Basin**

467 **4.3.1 Surface aerosol concentrations**

468 Figure 9 shows the time series of observed and simulated aerosol mass concentrations

469 at ATTO in January − June for the period of 2014 − 2016. Observed mean concentration

470 in wet season is 9.3 $\pm$ 7.6 µg m^{-3}, of which 83% is from coarse aerosol (7.7 µg m^{-3}),

471 while simulated concentration is 11 ± 6.7 μg m^{-3}, with dust contribution of 65% (7.2 μg

472 m^{-3}). The slight model bias could be to some extent explained by the difference in

473 background concentrations (1.9 and 5.1 μg m^{-3} for the observation and model data,

474 respectively). Most of observed peaks are found in February – March of 2014 and 2016,

475 and in February − April of 2015. The high correlation (r of $0.52 - 0.71$) between

476 observed coarse aerosols and simulated dust concentrations suggests that observed

477 strong variation in coarse aerosols is mainly driven by the influence of dust. Rizzolo et

478 al. (2017) conducted aerosol measurements at ATTO from 19 March to 24 April 2015.

479 The study showed the arrival of African dust between 3 and 6 April when the highest

480 concentrations of PM$_{10}$, soluble Fe (III) and Fe (II) were recorded at ATTO. The peak

481 value of 23 μg m^{-3} for PM$_{10}$ was observed on 5 April. This dust event is well reproduced

482 in this study with the peak value of 28 μg m^{-3} for PM$_{10}$ on the same day and the dust

483 contribution to PM$_{10}$ reaching above 70%. The co-occurrence of elevated sea salt

484 concentration (reaching 2.5 μg m^{-3}) during this event is also found in this study,

485 consistent with previous studies which show mixed transport of African dust and marine

486 aerosols to the basin (Wang et al., 2016; Ben-Ami et al., 2010; Rizzolo et al., 2017;

487 Adachi et al., 2020).

488 The dust peaks are generally associated with large dust emission and/or efficient

489 trans-Atlantic transport (e.g. relatively longer lifetime). For example, the relatively

490 higher dust concentrations in the wet season of 2015 (except for February) are

491 generally associated with higher emissions ($1.2 - 1.5$ Pg yr^{-1}) compared with the year

492 of 2014 and 2016 ($0.68 - 1.0$ Pg yr^{-1}, see Table S3). On the other hand, although

493 emissions in February 2016 (0.95 Pg yr^{-1}) is slightly lower than those in February

494 2014 (1.2 Pg yr^{-1}), the relatively longer lifetime (1.7 d vs. 1.5 d) may help explain the

495 relatively higher dust concentrations during that period. It should be noted that the

496 lifetime estimated here represents the export efficiency averaged over a relatively

497 large domain and a long-time scale (e.g. one month). Besides, the influence of African

498 dust on the ATTO site is also subject to the variations of transport paths and

499 precipitation fields.

500 Over the whole Amazon Basin, simulated mean surface dust concentrations in the wet

501 season of $2013 - 2017$ are 5.7 ± 1.3 μg m^{-3}, with a maximum of 7.9 μg m^{-3} in 2015

502 driven mainly by the relatively higher dust emission flux. The maxima of surface dust

503 concentrations are found in the northeast corner of the rainforest (over 15 µg m^{-3})

504 with a clearly decreasing trend towards southwestern direction (Figure 10). The dust

505 contribution to surface aerosol concentrations averaged over the whole basin is 40% ±

506 4.5%, again with the maximum of 48% found in 2015. The location with the largest

507 dust contributions (up to 70% in the north corner) slightly shifted inland compared to

508 the spatial distribution of dust concentrations. This could be explained by relatively

509 higher influence of sea salt aerosols along the coast (around 30-50% near the coast of

510 South America). Although the emission fluxes of both sea salt and dust are largely

511 determined by surface winds, the interannual variability of dust concentrations is

512 larger than sea salt over the Amazon Basin (20% vs. 10%) as the former is also

513 sensitive to the export efficiency across the Atlantic Ocean as discussed above.

514 Figure 10c also shows the frequency of dust events over the Amazon Basin, estimated

515 as the number of days when daily surface dust concentrations reaching the threshold

516 of 9 µg m^{-3} (Moran-Zuloaga et al., 2018) divided by the total number of days in the

517 wet season of 2013 − 2017. Dust frequency averaged over the whole region is around

518 18% ± 4.6% and decreases from 50 − 60% on the northeast coast to < 1% in southern

519 inland. The frequency of dust events at ATTO site is around 32%, close to the median

520 of the range. The interannual variation of the frequency (represented by RSD),

521 however, has an opposite trend, gradually increasing from 10% at the northeast coast

522 to over 100% in southern inland (36% at ATTO). During dust events, the dust mass

523 concentration at ATTO reaches 16 ± 2.9 µg m^{-3} (three times as high as that over the

524 whole wet season), accounting for around 75% ± 5.3% of total aerosol (Figure 10d).

525 Similarly, under the influence of the LRT of Saharan dust plumes, Moran-Zuloaga et

526 al. (2018) observed mass concentrations 14 ± 12 µg m^{-3} for coarse aerosol at the same

527 site, accounting for 93% of total observed aerosol.

528

4.3.2 AOD

530 The contribution of DOD to AOD at 550 nm over most areas of the Amazon Basin

531 (Figure 11) is in the range of 10 − 50% (23% ± 4.4% on average) during the wet

season of 2013 − 2017, with maxima in the northern Amazon Basin. The dust

contribution to total AOD is relatively smaller than that to surface aerosol

concentrations, mainly because of the relatively lower MEE of dust aerosols

compared to other aerosols. There also exists large difference in DOD between the

whole wet season and dust events: 0.021 ± 0.0055 vs. 0.055 ± 0.0076 averaged over

the Amazon Basin. A maximum of 0.31 on a daily basis is found on 1 Mar 2016 at the

northeast corner (55° W, 4° N) of the Amazon Basin during the study period. During

dust events, dust aerosols dominate AOD (40% − 60%) over most of the Amazon

Basin. At ATTO site, DOD is 0.034 ± 0.0088 and 0.063 ± 0.0087, accounting for 37%

and 53% of AOD during the whole wet season and dust events, respectively. The

largest dust contribution (up to 81%) with DOD of 0.18 at ATTO site is found on 24

Jan 2015. Consistent with our results, previous studies by Baars et al. (2011) and

Baars et al. (2012) reported an average AOD (532 nm) of ~0.14 when affected by the

influence of Saharan dust at a similar Amazon site (60° 2.3′ W, 2° 35.9′ S), during

which the DOD (532 nm) could be up to 0.18.

4.3.3 Dust deposition and related nutrient input

The spatial distribution of dust deposition over the Amazon Basin is also shown in

Figure 8. The mean dust deposition flux in the wet season is 2.0 ± 0.35 g m^{-2} yr^{-1},

much higher than in the dry season (August to November, 0.35 ± 0.16 g m^{-2} yr^{-1}). The

maximum (2.6 g m^{-2} yr^{-1}) is found in the year 2015 due to relatively large dust

emission and efficient trans-Atlantic transport. With emission of 0.96 ± 0.25 Pg yr^{-1} in

wet season (0.73 ± 0.12 Pg yr^{-1} on annual average), only 1.9% (1.4%) of African dust

is deposited into the Amazon Basin (dominated by wet deposition) while relatively

large part is deposited over the AOaTP (13% in the wet season and 14% on annual

average) and northern Africa (49% in the wet season).

Assuming mass fractions of 4.4%, 0.082%, and 1.8% for iron, phosphorus, and

magnesium respectively in African dust (Bristow et al., 2010; Chiemeka et al., 2007),

we derive deposition fluxes of 88 ± 15 mg m^{-2} yr^{-1}, 1.6 ± 0.29 mg m^{-2} yr^{-1} and 36 ± 6.3

561   mg m^{-2} yr^{-1} for iron, phosphorus and magnesium respectively into the Amazon

562   rainforest during the wet season and 52 ± 8.7, 0.97 ± 0.16 and 21 ± 3.6 mg m^{-2} yr^{-1} on

563   annual average (Figure 12). It should be noted that there exists large spatial variation

564   of nutrient input into the Amazon Basin associated with the patterns of dust deposition

565   flux. The deposition flux of iron during the wet season decreases from over 500 mg

566   m^{-2} yr^{-1} at the northeast coast to less than 15 mg m^{-2} yr^{-1} in the southwest and is above

567   50 mg m^{-2} yr^{-1} in most of the Amazon Basin. Similarly, the deposition flux decreases

568   from over 70 mg m^{-2} yr^{-1} (> 9 mg m^{-2} yr^{-1}) at the northeast coast to less than 7 mg

569   m^{-2} yr^{-1} (< 1 mg m^{-2} yr^{-1}) in inland for magnesium (phosphorus) during the wet

570   season. It seems that the nutrient input from Africa dust may play a significant role in

571   the northeastern part of the Amazon Basin, not in the southwest.

572   Table 4 summarized the estimates of dust and associated phosphorus deposition into

573   the Amazon Basin from previous studies. The estimated fluxes of dust and associated

574   phosphorus deposition are in the range of $0.81 - 19$ g m^{-2} yr^{-1} and $0.48 - 16$ mg m^{-2}

575   yr^{-1}. The large range is mainly driven by the high values (19 g m^{-2} yr^{-1} and 16 mg m^{-2}

576   yr^{-1} for dust and associated phosphorus, respectively) from the study of Swap et al.

577   (1992), which estimated dust importation into the northeastern basin, where it is most

578   subject to the intrusion of African dust. Besides the discrepancy in defined regions,

579   the wide range could also be partly explained by the application of different methods

580   and associated intrinsic uncertainties as mentioned in the Introduction. For instance,

581   the estimates from Swap et al. (1992) are mainly based on 1-month field

582   measurements at three sites located in the northeastern basin. Assumption about air

583   exchange rate across the coast to the basin, duration of dust storms as well as dust

584   concentrations contained in the dust plumes had to been made to extrapolate the dust

585   deposition into the Amazon Basin. Similarly, bias could also arise from insufficient

586   observations available to constrain models or satellite retrievals. Additional

587   uncertainty may also stem from the assumption about the P mass fraction, ranging

588   from 0.07% to 0.108%. Our results are similar to the finding of Prospero et al. (2020),

589   which has also been constrained by the observation at Cayenne site.

According to Salati and Vose (1984), the total amount of phosphorous and magnesium is 21.6 g m^{-2} and 29.8 g m^{-2}, respectively, in the ecosystem of the Amazon Basin (14.7 and 2.3 g m^{-2} respectively in the soil). Estimated nutrient input from African dust in our study accounts for 0.011% and 1.6% of total phosphorous and magnesium in the soil over the Amazon Basin during the wet season (0.0066% and 0.91% on annual average). On the other hand, Vitousek and Sanford (1986) reported a loss of $0.8 - 4$ mg m^{-2} yr^{-1} for phosphorus and 810 mg m^{-2} yr^{-1} for magnesium in Brazilian ecosystem to surface waters. Estimated annual phosphorous deposition flux of 0.97 ± 0.16 mg m^{-2} yr^{-1} into the Amazon Basin on average in our study is at the bottom end of the range of its hydrologic losses, implying that the nutrient input from African dust could to a large extent compensate the hydrologic losses of phosphorous in Brazilian forest ecosystem, although the deposition input of magnesium is much less than its hydrologic losses. Similarly, Abouchami et al. (2013) pointed out that most of the Amazonian rainforest is a system with an internal recycling of nutrients. But the extra influx of nutrients from African dust might account for a significant portion of the net ouflux, i.e. dissolved discharge of nutrients into rivers. Keep in mind that the estimates of nutrients influx are subject to the uncertainties in the estimates of dust flux as well as the mass fractions of nutrients containted in the dust. In addition, marine aerosols and biomassburning aerosols mixed with the LRT of African dust may also play a role for certain essential nutrients (Prospero et al., 2020; Abouchami et al., 2013). More observations including the nutrient mass fractions in African dust aerosols and the deposition fluxes of those elements into the Amazon Basin are necessarily required in the future work to better evaluate the nutrient input associated with the African dust intrusion.

5   Conclusion

In this study, we use the GEOS-Chem model with an optimized particle mass size distribution (PMSD) of dust aerosols to investigate the influence of the export of African dust towards the Amazon Basin during 2013 – 2017. The model performance

619   is constrained by multiple datasets obtained from AERONET, MODIS, as well as

620   Cayenne and ATTO sites in the Amazon Basin. The optimized PMSD in this study

621   well captures observed AOD regarding both the mean value as well as the decline rate

622   of the logarithm of AOD over the Atlantic Ocean along the transport path (AOaTP),

623   while the other two PMSD schemes tend to overestimate the decline rate by 11% and

624   underestimate the mean value by up to ~40%.

625   Simulated dust emission from northern Africa is 0.73 ± 0.12 Pg yr^{-1}, accounting for

626   more than 70% of global dust emission. There exists a strong seasonality in dust

627   emission with peaks in spring or winter, which varies with source regions. The

628   correlation analysis suggests high surface wind speeds and low soil moisture as a

629   major driver for dust emissions. In addition to the transport paths associated with the

630   oscillation of ITCZ, the export efficiency of African dust towards the Amazon basin is

631   sensitive to the removal of dust aerosol along the trans-Atlantic transport, which

632   depends on both assumed PMSD of dust aerosols in the model and meteorological

633   fields (i.e. precipitation and vertical transport path). The study further estimates the e-

634   folding lifetime of dust aerosols along the trans-Atlantic transport based on the

635   logarithm of the dust column burden against travel time over the AOaTP. The shortest

636   lifetime (1.4 d) is found for winter associated with high deposition flux, while the

637   highest dust burden over the AOaTP is found in summer mainly associated with its

638   longer lifetime (4.2 d).

639   Simulated surface dust concentration averaged over the whole Amazon Basin is $5.7 \pm$

640   1.3 µg m^{-3} during the wet season of 2013 – 2017, contributing $40\% \pm 4.5\%$ to total

641   surface aerosols. Observed dust peaks at the ATTO site are generally associated with

642   large dust emissions and/or efficient trans-Atlantic transport. The frequency of dust

643   events is $18\% \pm 4.6\%$ averaged over the Amazon Basin and up to $50\% - 60\%$ at the

644   northeast coast. During the dust events, DOD is around 0.055 ± 0.0076 and dominate

645   total AOD over most of the Amazon Basin. Associated with the deposition of African

646   dust, the study estimated annual inputs of 52 ± 8.7, 0.97 ± 0.16 and 21 ± 3.6 mg m^{-2}

647   yr^{-1} for iron, phosphorus, and magnesium, respectively, into the Amazon rainforest,

which may to some extent compensate the hydrologic losses of nutrients in the forest ecosystem.

Acknowledgements.

This work is supported by the National Natural Science Foundation of China (41907182, 41877303, 91644218), the National key R&D Program of China (2018YFC0213901), the Fundamental Research Funds for the Central Universities (21621105), the Guangdong Innovative and Entrepreneurial Research Team Program (Research team on atmospheric environmental roles and effects of carbonaceous species: 2016ZT06N263), and Special Fund Project for Science and Technology Innovation Strategy of Guangdong Province (2019B121205004). We acknowledge the support by the Instituto Nacional de Pesquisas da Amazônia (INPA). We would like to thank all people involved in the technical, logistical, and scientific support within the ATTO project.

Financial support. This work is supported by the National Natural Science Foundation of China (41907182, 41877303, 91644218), the National key R&D Program of China (2018YFC0213901), the Fundamental Research Funds for the Central Universities (21621105), the Guangdong Innovative and Entrepreneurial Research Team Program (Research team on atmospheric environmental roles and effects of carbonaceous species: 2016ZT06N263), and Special Fund Project for Science and Technology Innovation Strategy of Guangdong Province (2019B121205004). For the operation of the ATTO site, we acknowledge the support by the Max Planck Society (MPG), the German Federal Ministry of Education and Research (BMBF contracts 01LB1001A, 01LK1602B, and 01LK2101B) and the Brazilian Ministério da Ciência, Tecnologia e Inovação (MCTI/FINEP contract 01.11.01248.00), the Amazon State University (UEA), FAPEAM, LBA/INPA, FAPESP - Fundação de Amparo à Pesquisa do Estado de São Paulo, grant number 2017/17047-0, and SDS/CEUC/RDS-Uatumã. XW acknowledges the financial support of China Scholarship Council (CSC). MP acknowledges the financial support by the Max Planck Graduate Center with the Johannes-Gutenberg University, Mainz.

677 Author Contributions.

678 XRW conducted the data analysis, wrote the manuscript; QQW planned the study, collected

679 the resources, performed the model simulation and data analysis, and finalized the

680 manuscript; MP, CP, DM, and PA provided the observational data in the Amazon Basin, JWG,

681 NY, XJY, JCT, JH, NM, YFC and HS discussed the results; MA provided the observational

682 data in the Amazon Basin and reviewed the manuscript.

683

684 Competing interests.

685 Hang Su and Yafang Cheng are members of the editorial board of Atmospheric Chemistry and

686 Physics.

687

688 Data availability.

689 OPS data used in this study could be found at https://www.attodata.org/. Other datasets are

690 available upon request.

691

692 **References**

693 Abouchami, W., Näthe, K., Kumar, A., Galer, S. J. G., Jochum, K. P., Williams, E., Horbe, A.
694 M. C., Rosa, J. W. C., Balsam, W., Adams, D., Mezger, K., and Andreae, M. O.:
695 Geochemical and isotopic characterization of the Bodélé Depression dust source and
696 implications for transatlantic dust transport to the Amazon Basin, Earth Planet. Sc. Lett.,
697 380, 112-123, https://doi.org/10.1016/j.epsl.2013.08.028, 2013.
698 Adachi, K., Oshima, N., Gong, Z., de Sá, S., Bateman, A. P., Martin, S. T., de Brito, J. F.,
699 Artaxo, P., Cirino, G. G., Sedlacek Iii, A. J., and Buseck, P. R.: Mixing states of Amazon
700 basin aerosol particles transported over long distances using transmission electron
701 microscopy, Atmos. Chem. Phys., 20, 11923-11939, 10.5194/acp-20-11923-2020, 2020.
702 Alizadeh-Choobari, O., Sturman, A., and Zawar-Reza, P.: A global satellite view of the
703 seasonal distribution of mineral dust and its correlation with atmospheric circulation,
704 Dynam. Atmos. Oceans, 68, 20-34, https://doi.org/10.1016/j.dynatmoce.2014.07.002,
705 2014.
706 Andreae, M. O., Acevedo, O. C., Araùjo, A., Artaxo, P., Barbosa, C. G. G., Barbosa, H. M. J.,
707 Brito, J., Carbone, S., Chi, X., Cintra, B. B. L., da Silva, N. F., Dias, N. L., Dias-Júnior,
708 C. Q., Ditas, F., Ditz, R., Godoi, A. F. L., Godoi, R. H. M., Heimann, M., Hoffmann, T.,
709 Kesselmeier, J., Könemann, T., Krüger, M. L., Lavric, J. V., Manzi, A. O., Lopes, A. P.,
710 Martins, D. L., Mikhailov, E. F., Moran-Zuloaga, D., Nelson, B. W., Nölscher, A. C.,
711 Santos Nogueira, D., Piedade, M. T. F., Pöhlker, C., Pöschl, U., Quesada, C. A., Rizzo,
712 L. V., Ro, C. U., Ruckteschler, N., Sá, L. D. A., de Oliveira Sá, M., Sales, C. B., dos

Santos, R. M. N., Saturno, J., Schöngart, J., Sörgel, M., de Souza, C. M., de Souza, R. A. F., Su, H., Targhetta, N., Tóta, J., Trebs, I., Trumbore, S., van Eijck, A., Walter, D., Wang, Z., Weber, B., Williams, J., Winderlich, J., Wittmann, F., Wolff, S., and Yáñez-Serrano, A. M.: The Amazon Tall Tower Observatory (ATTO): overview of pilot measurements on ecosystem ecology, meteorology, trace gases, and aerosols, Atmos. Chem. Phys., 15, 10723-10776, 10.5194/acp-15-10723-2015, 2015.

Baars, H., Ansmann, A., Althausen, D., Engelmann, R., Artaxo, P., Pauliquevis, T., and Souza, R.: Further evidence for significant smoke transport from Africa to Amazonia, Geophys. Res. Lett., 38, https://doi.org/10.1029/2011GL049200, 2011.

Baars, H., Ansmann, A., Althausen, D., Engelmann, R., Heese, B., Müller, D., Artaxo, P., Paixao, M., Pauliquevis, T., and Souza, R.: Aerosol profiling with lidar in the Amazon Basin during the wet and dry season, J. Geophys. Res., 117, https://doi.org/10.1029/2012JD018338, 2012.

Bakker, N. L., Drake, N. A., and Bristow, C. S.: Evaluating the relative importance of northern African mineral dust sources using remote sensing, Atmos. Chem. Phys., 19, 10525-10535, 10.5194/acp-19-10525-2019, 2019.

Barkley, A. E., Prospero, J. M., Mahowald, N., Hamilton, D. S., Popendorf, K. J., Oehlert, A. M., Pourmand, A., Gatineau, A., Panechou-Pulcherie, K., Blackwelder, P., and Gaston, C. J.: African biomass burning is a substantial source of phosphorus deposition to the Amazon, Tropical Atlantic Ocean, and Southern Ocean, Proceedings of the National Academy of Sciences, 116, 16216-16221, 10.1073/pnas.1906091116, 2019.

Ben-Ami, Y., Koren, I., Altaratz, O., Kostinski, A., and Lehahn, Y.: Discernible rhythm in the spatio/temporal distributions of transatlantic dust, Atmos. Chem. Phys., 12, 2253-2262, 10.5194/acp-12-2253-2012, 2012.

Ben-Ami, Y., Koren, I., Rudich, Y., Artaxo, P., Martin, S. T., and Andreae, M. O.: Transport of North African dust from the Bodélé depression to the Amazon Basin: a case study, Atmos. Chem. Phys., 10, 7533-7544, 10.5194/acp-10-7533-2010, 2010.

Bristow, C. S., Hudson-Edwards, K. A., and Chappell, A.: Fertilizing the Amazon and equatorial Atlantic with West African dust, Geophys. Res. Lett., 37, https://doi.org/10.1029/2010GL043486, 2010.

Chen, Y., Kreidenweis, S. M., McInnes, L. M., Rogers, D. C., and DeMott, P. J.: Single particle analyses of ice nucleating aerosols in the upper troposphere and lower stratosphere, Geophys. Res. Lett., 25, 1391-1394, 10.1029/97gl03261, 1998.

Chiemeka, I. U., Oleka, M. O., and Chineke, T.: Determination of aerosol metal composition and concentration during the 2001/2002 Harmattan season at Uturu, Nigeria, Global J. Pure Appl. Sci., 13, 10.4314/gjpas.v13i3.16734, 2007.

Cowie, S. M., Knippertz, P., and Marsham, J. H.: A climatology of dust emission events from northern Africa using long-term surface observations, Atmos. Chem. Phys., 14, 8579-8597, 10.5194/acp-14-8579-2014, 2014.

Demott, P. J., Sassen, K., Poellot, M. R., Baumgardner, D., Rogers, D. C., Brooks, S. D., Prenni, A. J., and Kreidenweis, S. M.: African dust aerosols as atmospheric ice nuclei, Geophys. Res. Lett., 30, https://doi.org/10.1029/2003GL017410, 2003.

Di Biagio, C., Formenti, P., Balkanski, Y., Caponi, L., Cazaunau, M., Pangui, E., Journet, E., Nowak, S., Andreae, M. O., Kandler, K., Saeed, T., Piketh, S., Seibert, D., Williams, E.,

and Doussin, J. F.: Complex refractive indices and single-scattering albedo of global dust aerosols in the shortwave spectrum and relationship to size and iron content, Atmos. Chem. Phys., 19, 15503-15531, 10.5194/acp-19-15503-2019, 2019.

Drury, E., Jacob, D. J., Spurr, R. J. D., Wang, J., Shinozuka, Y., Anderson, B. E., Clarke, A. D., Dibb, J., McNaughton, C., and Weber, R.: Synthesis of satellite (MODIS), aircraft (ICARTT), and surface (IMPROVE, EPA-AQS, AERONET) aerosol observations over eastern North America to improve MODIS aerosol retrievals and constrain surface aerosol concentrations and sources, J. Geophys. Res., 115, https://doi.org/10.1029/2009JD012629, 2010.

Dubovik, O., Holben, B., Eck, T. F., Smirnov, A., Kaufman, Y. J., King, M. D., Tanré, D., and Slutsker, I.: Variability of Absorption and Optical Properties of Key Aerosol Types Observed in Worldwide Locations, J. Atmos. Sci., 59, 590-608, http://doi.org/10.1175/1520-0469(2002)059<0590:VOAAOP>2.0.CO;2, 2002.

Duncan Fairlie, T., Jacob, D. J., and Park, R. J.: The impact of transpacific transport of mineral dust in the United States, Atmos. Environ., 41, 1251-1266, https://doi.org/10.1016/j.atmosenv.2006.09.048, 2007.

Dusek, U., Frank, G. P., Hildebrandt, L., Curtius, J., Schneider, J., Walter, S., Chand, D., Drewnick, F., Hings, S., Jung, D., Borrmann, S., and Andreae, M. O.: Size Matters More Than Chemistry for Cloud-Nucleating Ability of Aerosol Particles, Science, 312, 1375-1378, doi:10.1126/science.1125261, 2006.

Enfield, D. B., Mestas-Nuñez, A. M., and Trimble, P. J.: The Atlantic Multidecadal Oscillation and its relation to rainfall and river flows in the continental U.S, Geophys. Res. Lett., 28, 2077-2080, https://doi.org/10.1029/2000GL012745, 2001.

Evan, A. T., Flamant, C., Gaetani, M., and Guichard, F.: The past, present and future of African dust, Nature, 531, 493-495, 10.1038/nature17149, 2016.

Formenti, P., Andreae, M. O., Lange, L., Roberts, G., Cafmeyer, J., Rajta, I., Maenhaut, W., Holben, B. N., Artaxo, P., and Lelieveld, J.: Saharan dust in Brazil and Suriname during the Large-Scale Biosphere-Atmosphere Experiment in Amazonia (LBA) - Cooperative LBA Regional Experiment (CLAIRE) in March 1998, J. Geophys. Res., 106, 14919-14934, 10.1029/2000JD900827, 2001.

Gläser, G., Wernli, H., Kerkweg, A., and Teubler, F.: The transatlantic dust transport from North Africa to the Americas—Its characteristics and source regions, Journal of Geophysical Research: Atmospheres, 120, 11,231-211,252, https://doi.org/10.1002/2015JD023792, 2015.

Herbert, R. J., Krom, M. D., Carslaw, K. S., Stockdale, A., Mortimer, R. J. G., Benning, L. G., Pringle, K., and Browse, J.: The Effect of Atmospheric Acid Processing on the Global Deposition of Bioavailable Phosphorus From Dust, Global Biogeochemical Cycles, 32, 1367-1385, https://doi.org/10.1029/2018GB005880, 2018.

Highwood, E. J., Haywood, J. M., Silverstone, M. D., Newman, S. M., and Taylor, J. P.: Radiative properties and direct effect of Saharan dust measured by the C-130 aircraft during Saharan Dust Experiment (SHADE): 2. Terrestrial spectrum, J. Geophys. Res., 108, https://doi.org/10.1029/2002JD002552, 2003.

Huneeus, N., Schulz, M., Balkanski, Y., Griesfeller, J., Prospero, J., Kinne, S., Bauer, S., Boucher, O., Chin, M., Dentener, F., Diehl, T., Easter, R., Fillmore, D., Ghan, S.,

Ginoux, P., Grini, A., Horowitz, L., Koch, D., Krol, M. C., Landing, W., Liu, X., Mahowald, N., Miller, R., Morcrette, J. J., Myhre, G., Penner, J., Perlwitz, J., Stier, P., Takemura, T., and Zender, C. S.: Global dust model intercomparison in AeroCom phase I, Atmos. Chem. Phys., 11, 7781-7816, 10.5194/acp-11-7781-2011, 2011.

Jaeglé, L., Quinn, P. K., Bates, T. S., Alexander, B., and Lin, J. T.: Global distribution of sea salt aerosols: new constraints from in situ and remote sensing observations, Atmos. Chem. Phys., 11, 3137-3157, 10.5194/acp-11-3137-2011, 2011.

Jimenez, J. L., Canagaratna, M. R., Donahue, N. M., Prevot, A. S. H., Zhang, Q., Kroll, J. H., DeCarlo, P. F., Allan, J. D., Coe, H., Ng, N. L., Aiken, A. C., Docherty, K. S., Ulbrich, I. M., Grieshop, A. P., Robinson, A. L., Duplissy, J., Smith, J. D., Wilson, K. R., Lanz, V. A., Hueglin, C., Sun, Y. L., Tian, J., Laaksonen, A., Raatikainen, T., Rautiainen, J., Vaattovaara, P., Ehn, M., Kulmala, M., Tomlinson, J. M., Collins, D. R., Cubison, M. J., Dunlea, J., Huffman, J. A., Onasch, T. B., Alfarra, M. R., Williams, P. I., Bower, K., Kondo, Y., Schneider, J., Drewnick, F., Borrmann, S., Weimer, S., Demerjian, K., Salcedo, D., Cottrell, L., Griffin, R., Takami, A., Miyoshi, T., Hatakeyama, S., Shimono, A., Sun, J. Y., Zhang, Y. M., Dzepina, K., Kimmel, J. R., Sueper, D., Jayne, J. T., Herndon, S. C., Trimborn, A. M., Williams, L. R., Wood, E. C., Middlebrook, A. M., Kolb, C. E., Baltensperger, U., and Worsnop, D. R.: Evolution of Organic Aerosols in the Atmosphere, Science, 326, 5959, 1525-1529, doi:10.1126/science.1180353, 2009.

Kaufman, Y. J.: Dust transport and deposition observed from the Terra-Moderate Resolution Imaging Spectroradiometer (MODIS) spacecraft over the Atlantic Ocean, Journal of Geophysical Research, 110, 10.1029/2003jd004436, 2005

Kim, D., Chin, M., Remer, L. A., Diehl, T., Bian, H., Yu, H., Brown, M. E., and Stockwell, W. R.: Role of surface wind and vegetation cover in multi-decadal variations of dust emission in the Sahara and Sahel, Atmos. Environ., 148, 282-296, https://doi.org/10.1016/j.atmosenv.2016.10.051, 2017.

Kim, D., Chin, M., Yu, H., Diehl, T., Tan, Q., Kahn, R. A., Tsigaridis, K., Bauer, S. E., Takemura, T., Pozzoli, L., Bellouin, N., Schulz, M., Peyridieu, S., Chédin, A., and Koffi, B.: Sources, sinks, and transatlantic transport of North African dust aerosol: A multimodel analysis and comparison with remote sensing data, J. Geophys. Res., 119, 6259-6277, https://doi.org/10.1002/2013JD021099, 2014.

Knippertz, P., Deutscher, C., Kandler, K., Müller, T., Schulz, O., and Schütz, L.: Dust mobilization due to density currents in the Atlas region: Observations from the Saharan Mineral Dust Experiment 2006 field campaign, J. Geophys. Res., 112, https://doi.org/10.1029/2007JD008774, 2007.

Koepke, P., Hess, M., Schult, I., and Shettle, E. P.: Global aerosol data set, Max-Planck Institute for Meteorology, 44, 1997.

Kok, J. F.: A scaling theory for the size distribution of emitted dust aerosols suggests climate models underestimate the size of the global dust cycle, Proc Natl Acad Sci U S A, 108, 1016-1021, 10.1073/pnas.1014798108, 2011.

Kok, J. F., Adebiyi, A. A., Albani, S., Balkanski, Y., Checa-Garcia, R., Chin, M., Colarco, P. R., Hamilton, D. S., Huang, Y., Ito, A., Klose, M., Li, L., Mahowald, N. M., Miller, R. L., Obiso, V., Pérez García-Pando, C., Rocha-Lima, A., and Wan, J. S.: Contribution of the world's main dust source regions to the global cycle of desert dust, Atmos. Chem.

845   Phys., 21, 8169-8193, 10.5194/acp-21-8169-2021, 2021.

846 Li, Y., Randerson, J. T., Mahowald, N. M., and Lawrence, P. J.: Deforestation Strengthens

847   Atmospheric Transport of Mineral Dust and Phosphorus from North Africa to the

848   Amazon, Journal of Climate, 34, 6087-6096, 10.1175/jcli-d-20-0786.1, 2021.

849 Liu, D., Taylor, J. W., Crosier, J., Marsden, N., Bower, K. N., Lloyd, G., Ryder, C. L., Brooke,

850   J. K., Cotton, R., Marenco, F., Blyth, A., Cui, Z., Estelles, V., Gallagher, M., Coe, H., and

851   Choularton, T. W.: Aircraft and ground measurements of dust aerosols over the west

852   African coast in summer 2015 during ICE-D and AER-D, Atmos. Chem. Phys., 18,

853   3817-3838, 10.5194/acp-18-3817-2018, 2018.

854 Liu, H., Jacob, D. J., Bey, I., and Yantosca, R. M.: Constraints from 210Pb and 7Be on wet

855   deposition and transport in a global three-dimensional chemical tracer model driven by

856   assimilated meteorological fields, J. Geophys. Res., 106, 12109-12128,

857   https://doi.org/10.1029/2000JD900839, 2001.

858 Lucchesi, R.: File Specification for GEOS-5 FP, GMAO Office Note No.4 (Version 1.0), 63

859   pp., available at: http://gmao.gsfc.nasa.gov/pubs/office_notes, 2013.

860 Mahowald, N., Albani, S., Engelstaedter, S., Winckler, G., and Goman, M.: Model insight into

861   glacial–interglacial paleodust records, Quaterny Sci. Rev., 30, 832-854,

862   https://doi.org/10.1016/j.quascirev.2010.09.007, 2011a.

863 Mahowald, N., Albani, S., Kok, J. F., Engelstaeder, S., Scanza, R., Ward, D. S., and Flanner,

864   M. G.: The size distribution of desert dust aerosols and its impact on the Earth system,

865   Aeolian Res., 15, 53-71, https://doi.org/10.1016/j.aeolia.2013.09.002, 2014.

866 Mahowald, N. M., Artaxo, P., Baker, A. R., Jickells, T. D., Okin, G. S., Randerson, J. T., and

867   Townsend, A. R.: Impacts of biomass burning emissions and land use change on

868   Amazonian atmospheric phosphorus cycling and deposition, Global Biogeochemical

869   Cycles, 19, https://doi.org/10.1029/2005GB002541, 2005.

870 Mahowald, N., Ward, D. S., Kloster, S., Flanner, M. G., Heald, C. L., Heavens, N. G., Hess, P.

871   G., Lamarque, J.-F., and Chuang, P. Y.: Aerosol Impacts on Climate and

872   Biogeochemistry, Annu. Rev. Env. Resour., 36, 45-74, 10.1146/annurev-environ-042009-

873   094507, 2011b.

874 Mahowald, N. M. and Kiehl, L. M.: Mineral aerosol and cloud interactions, Geophys. Res.

875   Lett., 30, https://doi.org/10.1029/2002GL016762, 2003.

876 Mahowald, N. M., Muhs, D. R., Levis, S., Rasch, P. J., Yoshioka, M., Zender, C. S., and Luo,

877   C.: Change in atmospheric mineral aerosols in response to climate: Last glacial period,

878   preindustrial, modern, and doubled carbon dioxide climates, J. Geophys. Res., 111,

879   https://doi.org/10.1029/2005JD006653, 2006.

880 Martin, R. V., Jacob, D. J., Yantosca, R. M., Chin, M., and Ginoux, P.: Global and regional

881   decreases in tropospheric oxidants from photochemical effects of aerosols, J. Geophys.

882   Res. , 108, https://doi.org/10.1029/2002JD002622, 2003.

883 Martin, S. T., Andreae, M. O., Artaxo, P., Baumgardner, D., Chen, Q., Goldstein, A. H.,

884   Guenther, A., Heald, C. L., Mayol-Bracero, O. L., McMurry, P. H., Pauliquevis, T.,

885   Pöschl, U., Prather, K. A., Roberts, G. C., Saleska, S. R., Silva Dias, M. A., Spracklen,

886   D. V., Swietlicki, E., and Trebs, I.: Sources and properties of Amazonian aerosol

887   particles, Rev. Geophys., 48, https://doi.org/10.1029/2008RG000280, 2010a.

888 Martin, S. T., Andreae, M. O., Althausen, D., Artaxo, P., Baars, H., Borrmann, S., Chen, Q.,

Farmer, D. K., Guenther, A., Gunthe, S. S., Jimenez, J. L., Karl, T., Longo, K., Manzi, A., Müller, T., Pauliquevis, T., Petters, M. D., Prenni, A. J., Pöschl, U., Rizzo, L. V., Schneider, J., Smith, J. N., Swietlicki, E., Tota, J., Wang, J., Wiedensohler, A., and Zorn, S. R.: An overview of the Amazonian Aerosol Characterization Experiment 2008 (AMAZE-08), Atmos. Chem. Phys., 10, 11415-11438, 10.5194/acp-10-11415-2010, 2010b.

Middleton, N.: Variability and Trends in Dust Storm Frequency on Decadal Timescales: Climatic Drivers and Human Impacts, Geosciences, 9, 261, http://doi.org/10.3390/geosciences9060261, 2019.

Moran-Zuloaga, D., Ditas, F., Walter, D., Saturno, J., Brito, J., Carbone, S., Chi, X., Hrabě de Angelis, I., Baars, H., Godoi, R. H. M., Heese, B., Holanda, B. A., Lavrič, J. V., Martin, S. T., Ming, J., Pöhlker, M. L., Ruckteschler, N., Su, H., Wang, Y., Wang, Q., Wang, Z., Weber, B., Wolff, S., Artaxo, P., Pöschl, U., Andreae, M. O., and Pöhlker, C.: Long-term study on coarse mode aerosols in the Amazon rain forest with the frequent intrusion of Saharan dust plumes, Atmos. Chem. Phys., 18, 10055-10088, 10.5194/acp-18-10055-2018, 2018.

Niedermeier, N., Held, A., Müller, T., Heinold, B., Schepanski, K., Tegen, I., Kandler, K., Ebert, M., Weinbruch, S., Read, K., Lee, J., Fomba, K. W., Müller, K., Herrmann, H., and Wiedensohler, A.: Mass deposition fluxes of Saharan mineral dust to the tropical northeast Atlantic Ocean: an intercomparison of methods, Atmos. Chem. Phys., 14, 2245-2266, 10.5194/acp-14-2245-2014, 2014.

Pöhlker, C., Walter, D., Paulsen, H., Könemann, T., Rodríguez-Caballero, E., Moran-Zuloaga, D., Brito, J., Carbone, S., Degrendele, C., Després, V. R., Ditas, F., Holanda, B. A., Kaiser, J. W., Lammel, G., Lavrič, J. V., Ming, J., Pickersgill, D., Pöhlker, M. L., Praß, M., Löbs, N., Saturno, J., Sörgel, M., Wang, Q., Weber, B., Wolff, S., Artaxo, P., Pöschl, U., and Andreae, M. O.: Land cover and its transformation in the backward trajectory footprint region of the Amazon Tall Tower Observatory, Atmos. Chem. Phys., 19, 8425-8470, 10.5194/acp-19-8425-2019, 2019.

Pöhlker, M. L., Ditas, F., Saturno, J., Klimach, T., Hrabě de Angelis, I., Araùjo, A. C., Brito, J., Carbone, S., Cheng, Y., Chi, X., Ditz, R., Gunthe, S. S., Holanda, B. A., Kandler, K., Kesselmeier, J., Könemann, T., Krüger, O. O., Lavrič, J. V., Martin, S. T., Mikhailov, E., Moran-Zuloaga, D., Rizzo, L. V., Rose, D., Su, H., Thalman, R., Walter, D., Wang, J., Wolff, S., Barbosa, H. M. J., Artaxo, P., Andreae, M. O., Pöschl, U., and Pöhlker, C.: Long-term observations of cloud condensation nuclei over the Amazon rain forest – Part 2: Variability and characteristics of biomass burning, long-range transport, and pristine rain forest aerosols, Atmos. Chem. Phys., 18, 10289-10331, 10.5194/acp-18-10289-2018, 2018.

Pöschl, U., Martin, S. T., Sinha, B., Chen, Q., Gunthe, S. S., Huffman, J. A., Borrmann, S., Farmer, D. K., Garland, R. M., Helas, G., Jimenez, J. L., King, S. M., Manzi, A., Mikhailov, E., Pauliquevis, T., Petters, M. D., Prenni, A. J., Roldin, P., Rose, D., Schneider, J., Su, H., Zorn, S. R., Artaxo, P., and Andreae, M. O.: Rainforest Aerosols as Biogenic Nuclei of Clouds and Precipitation in the Amazon, Science, 329, 1513-1516, doi:10.1126/science.1191056, 2010.

Prass, M., Andreae, M. O., de Araùjo, A. C., Artaxo, P., Ditas, F., Elbert, W., Förster, J. D.,

Franco, M. A., Hrabe de Angelis, I., Kesselmeier, J., Klimach, T., Kremper, L. A., Thines, E., Walter, D., Weber, J., Weber, B., Fuchs, B. M., Pöschl, U., and Pöhlker, C.: Bioaerosols in the Amazon rain forest: temporal variations and vertical profiles of Eukarya, Bacteria, and Archaea, Biogeosciences, 18, 4873-4887, 10.5194/bg-18-4873-2021, 2021.

Prospero, J. M., Glaccum, R. A., and Nees, R. T.: Atmospheric transport of soil dust from Africa to South America, Nature, 289, 570-572, 10.1038/289570a0, 1981.

Prospero, J. M., Collard, F.-X., Molinié, J., and Jeannot, A.: Characterizing the annual cycle of African dust transport to the Caribbean Basin and South America and its impact on the environment and air quality, Global Biogeochem. Cy., 28, 757-773, https://doi.org/10.1002/2013GB004802, 2014.

Prospero, J. M., Barkley, A. E., Gaston, C. J., Gatineau, A., Campos y Sansano, A., and Panechou, K.: Characterizing and Quantifying African Dust Transport and Deposition to South America: Implications for the Phosphorus Budget in the Amazon Basin, Global Biogeochem. Cy., 34, e2020GB006536, https://doi.org/10.1029/2020GB006536, 2020.

Ridley, D. A., Heald, C. L., and Ford, B.: North African dust export and deposition: A satellite and model perspective, J. Geophys. Res., 117, https://doi.org/10.1029/2011JD016794, 2012.

Ridley, D. A., Heald, C. L., and Prospero, J. M.: What controls the recent changes in African mineral dust aerosol across the Atlantic?, Atmos. Chem. Phys., 14, 5735-5747, 10.5194/acp-14-5735-2014, 2014.

Rizzolo, J. A., Barbosa, C. G. G., Borillo, G. C., Godoi, A. F. L., Souza, R. A. F., Andreoli, R. V., Manzi, A. O., Sá, M. O., Alves, E. G., Pöhlker, C., Angelis, I. H., Ditas, F., Saturno, J., Moran-Zuloaga, D., Rizzo, L. V., Rosário, N. E., Pauliquevis, T., Santos, R. M. N., Yamamoto, C. I., Andreae, M. O., Artaxo, P., Taylor, P. E., and Godoi, R. H. M.: Soluble iron nutrients in Saharan dust over the central Amazon rainforest, Atmos. Chem. Phys., 17, 2673-2687, 10.5194/acp-17-2673-2017, 2017.

Roberts, A. and Knippertz, P.: Haboobs: Convectively generated dust storms in West Africa, Weather, 67, 311 - 316, 2012.

Ryder, C. L., Highwood, E. J., Lai, T. M., Sodemann, H., and Marsham, J. H.: Impact of atmospheric transport on the evolution of microphysical and optical properties of Saharan dust, Geophys. Res. Lett., 40, 2433-2438, 10.1002/grl.50482, 2013a.

Ryder, C. L., Highwood, E. J., Rosenberg, P. D., Trembath, J., Brooke, J. K., Bart, M., Dean, A., Crosier, J., Dorsey, J., Brindley, H., Banks, J., Marsham, J. H., McQuaid, J. B., Sodemann, H., and Washington, R.: Optical properties of Saharan dust aerosol and contribution from the coarse mode as measured during the Fennec 2011 aircraft campaign, Atmos. Chem. Phys., 13, 303-325, 10.5194/acp-13-303-2013, 2013b.

Ryder, C. L., Marenco, F., Brooke, J. K., Estelles, V., Cotton, R., Formenti, P., McQuaid, J. B., Price, H. C., Liu, D., Ausset, P., Rosenberg, P. D., Taylor, J. W., Choularton, T., Bower, K., Coe, H., Gallagher, M., Crosier, J., Lloyd, G., Highwood, E. J., and Murray, B. J.: Coarse-mode mineral dust size distributions, composition and optical properties from AER-D aircraft measurements over the tropical eastern Atlantic, Atmos. Chem. Phys., 18, 17225-17257, 10.5194/acp-18-17225-2018, 2018.

Salati, E. and Vose, P. B.: Amazon Basin: A System in Equilibrium, Science, 225, 129-138,

977   doi:10.1126/science.225.4658.129, 1984.

978 Shao, Y., Fink, A. H., and Klose, M.: Numerical simulation of a continental-scale Saharan
979   dust event, J. Geophys. Res., 115, https://doi.org/10.1029/2009JD012678, 2010.

980 Shao, Y., Klose, M., and Wyrwoll, K.-H.: Recent global dust trend and connections to climate
981   forcing, J. Geophys. Res., 118, 11,107-111,118, https://doi.org/10.1002/jgrd.50836,
982   2013.

983 Sinyuk, A., Torres, O., and Dubovik, O.: Combined use of satellite and surface observations
984   to infer the imaginary part of refractive index of Saharan dust, Geophys. Res. Lett., 30,
985   https://doi.org/10.1029/2002GL016189, 2003.

986 SWAP, R., GARSTANG, M., GRECO, S., TALBOT, R., and KÅLLBERG, P.: Saharan dust
987   in the Amazon Basin, Tellus B, 44, 133-149, https://doi.org/10.1034/j.1600-
988   0889.1992.t01-1-00005.x, 1992.

989 Talbot, R. W., Andreae, M. O., Berresheim, H., Artaxo, P., Garstang, M., Harriss, R. C.,
990   Beecher, K. M., and Li, S. M.: Aerosol chemistry during the wet season in central
991   Amazonia: The influence of long-range transport, J. Geophys. Res., 95, 16955-16969,
992   https://doi.org/10.1029/JD095iD10p16955, 1990.

993 van der Does, M., Korte, L. F., Munday, C. I., Brummer, G. J. A., and Stuut, J. B. W.: Particle
994   size traces modern Saharan dust transport and deposition across the equatorial North
995   Atlantic, Atmos. Chem. Phys., 16, 13697-13710, 10.5194/acp-16-13697-2016, 2016.

996 Vitousek, P. M. and Sanford, R. L.: Nutrient Cycling in Moist Tropical Forest, Annual Review
997   of Ecology and Systematics, 17, 137-167, http://www.jstor.org/stable/2096992.1986.

998 Wang, J., Christopher, S. A., Brechtel, F., Kim, J., Schmid, B., Redemann, J., Russell, P. B.,
999   Quinn, P., and Holben, B. N.: Geostationary satellite retrievals of aerosol optical
1000   thickness during ACE-Asia, J. Geophys. Res., 108,
1001   https://doi.org/10.1029/2003JD003580, 2003a.

1002 Wang, J., Christopher, S. A., Reid, J. S., Maring, H., Savoie, D., Holben, B. N., Livingston, J.
1003   M., Russell, P. B., and Yang, S.-K.: GOES 8 retrieval of dust aerosol optical thickness
1004   over the Atlantic Ocean during PRIDE, J. Geophys. Res., 108,
1005   https://doi.org/10.1029/2002JD002494, 2003b.

1006 Wang, Q., Gu, J., and Wang, X.: The impact of Sahara dust on air quality and public health in
1007   European countries, Atmospheric Environment, 241, 117771,
1008   https://doi.org/10.1016/j.atmosenv.2020.117771, 2020.

1009 Wang, Q., Jacob, D. J., Fisher, J. A., Mao, J., Leibensperger, E. M., Carouge, C. C., Le Sager,
1010   P., Kondo, Y., Jimenez, J. L., Cubison, M. J., and Doherty, S. J.: Sources of carbonaceous
1011   aerosols and deposited black carbon in the Arctic in winter-spring: implications for
1012   radiative forcing, Atmos. Chem. Phys., 11, 12453-12473, 10.5194/acp-11-12453-2011,
1013   2011.

1014 Wang, Q., Saturno, J., Chi, X., Walter, D., Lavric, J. V., Moran-Zuloaga, D., Ditas, F., Pöhlker,
1015   C., Brito, J., Carbone, S., Artaxo, P., and Andreae, M. O.: Modeling investigation of
1016   light-absorbing aerosols in the Amazon Basin during the wet season, Atmos. Chem.
1017   Phys., 16, 14775-14794, 10.5194/acp-16-14775-2016, 2016.

1018 Wang, W., Evan, A. T., Lavaysse, C., and Flamant, C.: The role the Saharan Heat Low plays
1019   in dust emission and transport during summertime in North Africa, Aeolian Res., 28, 1-
1020   12, https://doi.org/10.1016/j.aeolia.2017.07.001, 2017.

Wang, Y., Jacob, D. J., and Logan, J. A.: Global simulation of tropospheric O3-NO x - hydrocarbon chemistry: 1. Model formulation, J. Geophys. Res. , 103, 10713-10725, https://doi.org/10.1029/98JD00158, 1998.

Wesely, M. L.: Parameterization of surface resistances to gaseous dry deposition in regional-scale numerical models, Atmos. Environ., 41, 52-63, https://doi.org/10.1016/j.atmosenv.2007.10.058, 2007.

White, B. R.: soil transport by winds on Mars, Journal of Geophysical Research: Solid Earth, 84, 4643-4651, https://doi.org/10.1029/JB084iB09p04643, 1979.

Wu, L., Li, X., Kim, H., Geng, H., Godoi, R. H. M., Barbosa, C. G. G., Godoi, A. F. L., Yamamoto, C. I., de Souza, R. A. F., Pöhlker, C., Andreae, M. O., and Ro, C. U.: Single-particle characterization of aerosols collected at a remote site in the Amazonian rainforest and an urban site in Manaus, Brazil, Atmos. Chem. Phys., 19, 1221-1240, 10.5194/acp-19-1221-2019, 2019.

Ysard, N., Jones, A. P., Demyk, K., Boutéraon, T., and Koehler, M.: The optical properties of dust: the effects of composition, size, and structure, A&A, 617, A124, 2018.

Yu, H., Chin, M., Bian, H., Yuan, T., Prospero, J. M., Omar, A. H., Remer, L. A., Winker, D. M., Yang, Y., Zhang, Y., and Zhang, Z.: Quantification of trans-Atlantic dust transport from seven-year (2007–2013) record of CALIPSO lidar measurements, Remote Sens. Environ., 159, 232-249, https://doi.org/10.1016/j.rse.2014.12.010, 2015a.

Yu, H., Chin, M., Yuan, T., Bian, H., Remer, L. A., Prospero, J. M., Omar, A., Winker, D., Yang, Y., Zhang, Y., Zhang, Z., and Zhao, C.: The fertilizing role of African dust in the Amazon rainforest: A first multiyear assessment based on data from Cloud-Aerosol Lidar and Infrared Pathfinder Satellite Observations, Geophys. Res. Lett., 42, 1984-1991, 10.1002/2015GL063040, 2015b.

Yu, Y., Kalashnikova, O. V., Garay, M. J., Lee, H., Notaro, M., Campbell, J. R., Marquis, J., Ginoux, P., and Okin, G. S.: Disproving the Bodélé Depression as the Primary Source of Dust Fertilizing the Amazon Rainforest, Geophysical Research Letters, 47, 2020.

Yu, H., Tan, Q., Chin, M., Remer, L. A., Kahn, R. A., Bian, H., Kim, D., Zhang, Z., Yuan, T., Omar, A. H., Winker, D. M., Levy, R. C., Kalashnikova, O., Crepeau, L., Capelle, V., and Chédin, A.: Estimates of African Dust Deposition Along the Trans-Atlantic Transit Using the Decadelong Record of Aerosol Measurements from CALIOP, MODIS, MISR, and IASI, J. Geophys. Res., 124, 7975-7996, https://doi.org/10.1029/2019JD030574, 2019.

Yuan, T., Yu, H., Chin, M., Remer, L. A., McGee, D., and Evan, A.: Anthropogenic Decline of African Dust: Insights From the Holocene Records and Beyond, Geophys. Res. Lett., 47, e2020GL089711, https://doi.org/10.1029/2020GL089711, 2020.

Zender, C. S., Bian, H., and Newman, D.: Mineral Dust Entrainment and Deposition (DEAD) model: Description and 1990s dust climatology, J. Geophys. Res., 108, https://doi.org/10.1029/2002JD002775, 2003.

Zhang, L., Gong, S., Padro, J., and Barrie, L.: A size-segregated particle dry deposition scheme for an atmospheric aerosol module, Atmos. Environ., 35, 549-560, https://doi.org/10.1016/S1352-2310(00)00326-5, 2001.

Zhang, L., Kok, J. F., Henze, D. K., Li, Q., and Zhao, C.: Improving simulations of fine dust surface concentrations over the western United States by optimizing the particle size distribution, Geophys. Res. Lett., 40, 3270-3275, 10.1002/grl.50591, 2013.

1065

Table 1. Mass fractions (%) of dust emitted in each bin for different particle mass size distribution (PMSD) schemes tested in GEOS-Chem.

| Scheme | bin 1 | | | | bin 2 | bin 3 | bin 4 |
	sub-bin 1 (0.1 – 0.18)[a] (3.1)[b]	sub-bin 2 (0.18 – 0.3)[a] (4.3)[b]	sub-bin 3 (0.3 – 0.6)[a] (2.7)[b]	sub-bin 4 (0.6 – 1.0)[a] (0.96)[b]	(1.0 – 1.8)[a] (0.45)[b]	(1.8 – 3.0)[a] (0.27)[b]	(3.0 – 6.0)[a] (0.16)[b]
V12	0.7	3.32	24.87	71.11	19.2	34.9	38.2
		(bin 1 total: 7.7)					
V12_C	6	12	24	58.00	25.3	32.2	30.2
		(bin 1 total: 12.2)					
V12_F	3.9	8.06	43	45.04	11.9	15.6	67
		(bin 1 total: 5.5)					

[a] size range in radius (μm) for each bin

[b] mass extinction efficiency (MEE) at wavelength of 550 nm in unit of $m^2\ g^{-1}$ for dust particles in each bin in the GEOS-Chem mod

Table 2. Summary of the observations used in this study, including the parameters, the spatio-temporal coverage, and the corresponding application in the model.

Datasets	Parameters	Locations	Periods (resolution)	Application
AERONET	AOD	northern Africa, the Atlantic Ocean	2013 – 2017 (daily)	Model AOD evaluation over northern Africa and the Atlantic Ocean
	PVSD[a]	northern Africa	2013 – 2017 (daily)	Model dust PMSD evaluation
Fennec Campaign	PMSD[b]	Over Mali and Algeria, Africa	17 – 28 June, 2011	Model dust PMSD evaluation
MODIS	AOD	northern Africa and the Atlantic Ocean	2013 – 2017 (daily)	Model AOD evaluation over northern Africa and the Atlantic Ocean
Cayenne	PM_{10}	52.3097° W, 4.9489° N (France)	January – April, 2014 (daily)	Model dust mass concentration evaluation at the coast of South America
ATTO	PNSD[c]	59.0056° W, 2.1459° S (Brazil)	January – April, 2014 – 2016 (5 min)	Model dust mass concentration evaluation at the central Amazon Basin

[a] particle volume size distribution; [b] particle mass size distribution; [c] particle number size distribution

Table 3. Annual and seasonal dust emissions (Pg yr^{-1}) in northern Africa (17.5° W –

40° E, 10° N – 35° N)[a] simulated in GEOS-Chem.

Year	Spring	Summer	Fall	Winter	Annual (Wet season)
2013	1.2	0.77	0.48	1.0	0.88 (1.1)
2014	0.83	0.84	0.51	0.91	0.77 (0.89)
2015	1.2	0.46	0.33	1.1	0.77 (1.3)
2016	0.82	0.52	0.37	0.89	0.65 (0.86)
2017	0.68	0.38	0.47	0.70	0.56 (0.63)
Mean±std[b]	0.95±0.24	0.59±0.20	0.43±0.078	0.92±0.15	0.73±0.12 (0.96±0.25)

[a] Spring: March – May; Summer: June – August; Fall: September – November; Winter: January,

February, and December; Wet season: January – April

[b] standard deviation

Table 4. Estimates of annual dust and associated phosphorus deposition into the

Amazon Basin.

Methods	Dust deposition		P deposition		References
	total	flux	total	flux	
	(Tg a^{-1})	(g m^{-2} a^{-1})	(Tg a^{-1})	(mg m^{-2} a^{-1})	
CESM2	10 ± 2.1	n/a	0.0077±0.0016	n/a	Li et al. (2021)[a]
AeroCom Phase I	7.7	0.81	0.0063	0.66	Kok et al. (2021)[b]
MERRA-2	8.0	1.05	0.0062	0.9	Prospero et al. (2020)[a]
MERRA-2, CAM	n/a	n/a	0.011 – 0.033	1.1 – 3.5	Barkley et al. (2019)[a]
GLOMAP	32	1.8	0.019	1.1	Herbert et al. (2018)[a]
CALIOP	8– 48	0.8 – 5	0.006 – 0.037	0.7 – 3.9	Yu et al. (2015b)[a]
ECHAM5	30.3/11.4	n/a	0.025/0.0093	n/a	Gläser et al. (2015)[b]
GEOS-Chem	17± 5	n/a	0.014	n/a	Ridley et al. (2012)[b]
MATCH	n/a	n/a	n/a	0.48	Mahowald et al. (2005)[a]
MODIS	50	n/a	0.041	n/a	Kaufman (2005)[b]
Field measurement	13	19	0.011	16	Swap et al. (1992)[b]

| GEOS-Chem | 10 ± 1.7 | 1.2 ± 0.20 | 0.0085 ± 0.0014 | 0.97 ± 0.16 | This study |

1085   *Note*. Table extracted in part from Prospero et al. (2020).

1086   [a] The P mass fraction is 0.077% for Li et al. (2021) and Prospero et al. (2020), 0.108% for Barkley

1087   et al. (2019), 0.088% for Herbert et al. (2018), 0.078% for Yu et al. (2015b), and 0.07% for

1088   Mahowald et al. (2005).

1089   [b] Assuming P mass fraction of 0.082% in dust, the same value as used in this study.

1090

1091

1092

1093

1094

1095

1096

1097
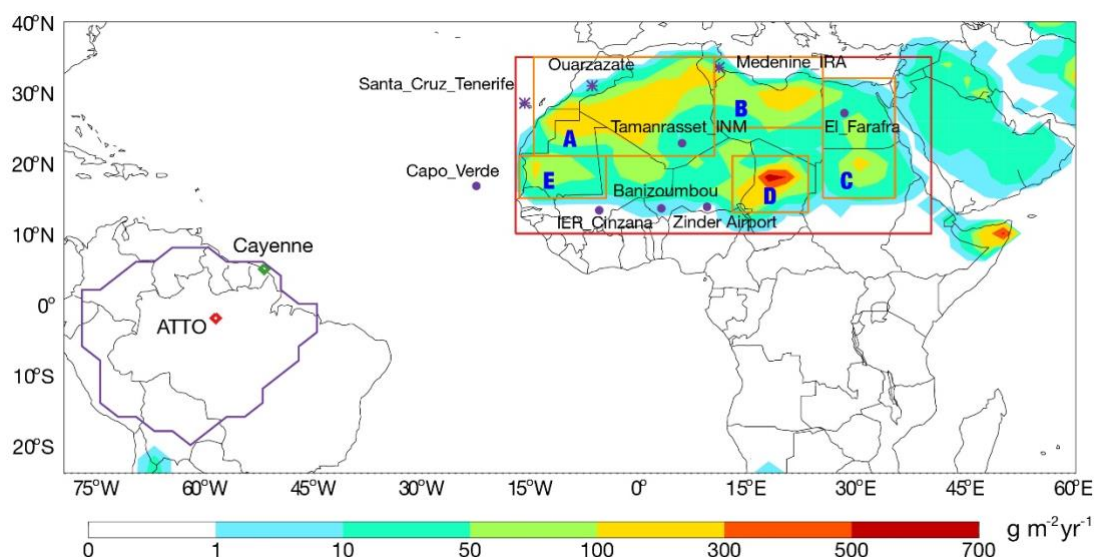
1098

1099   **Figure 1.** Simulated annual dust emissions in GEOS-Chem, averaged from 2013 to 2017. The

1100   location of AERONET sites used in Figure 2 are marked as purple symbols, of which circles

1101   represent the sites used in Figure 3. The region of the Amazon Basin is defined by purple lines.

1102   The location of Cayenne site in the northeast coast of South America and ATTO site in the

1103   central Amazon Basin are marked as green and red diamonds, respectively. The red rectangle

1104   illustrates the area of northern Africa (17.5° W – 40° E, 10° N – 35° N) and the orange

1105   rectangles shows the areas of five major source regions described in the text (A: 15° W – 10°

1106   E, 21° N – 35° N; B: 10° E – 25° E, 25° N – 35°N; C: 25° E – 35° E, 15° N – 32° N; D: 12.5°

1107   E – 23° E, 13° N – 21° N; E: 17° W – 5°W, 15° N – 21° N).

1108

1109
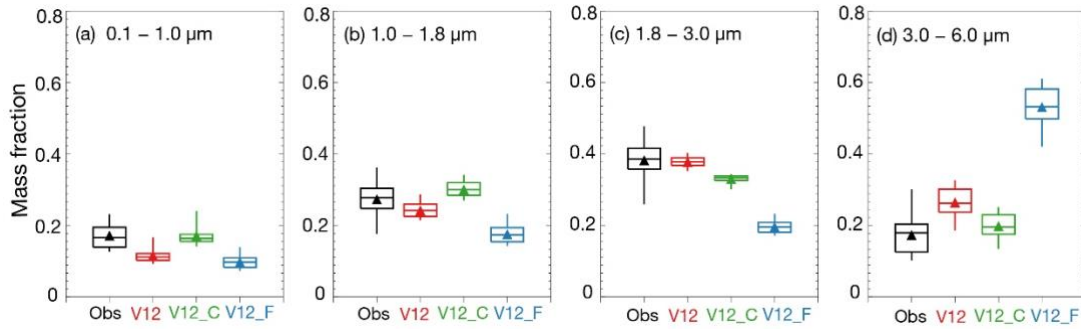
1110

1111 **Figure 2.** Boxplots of the mass fractions of column-integrated aerosols in the four size bins (in

1112 radius) retrieved from AERONET sites over Africa compared with model results based on different

1113 PMSD schemes. The triangles represent the mean values.

1114
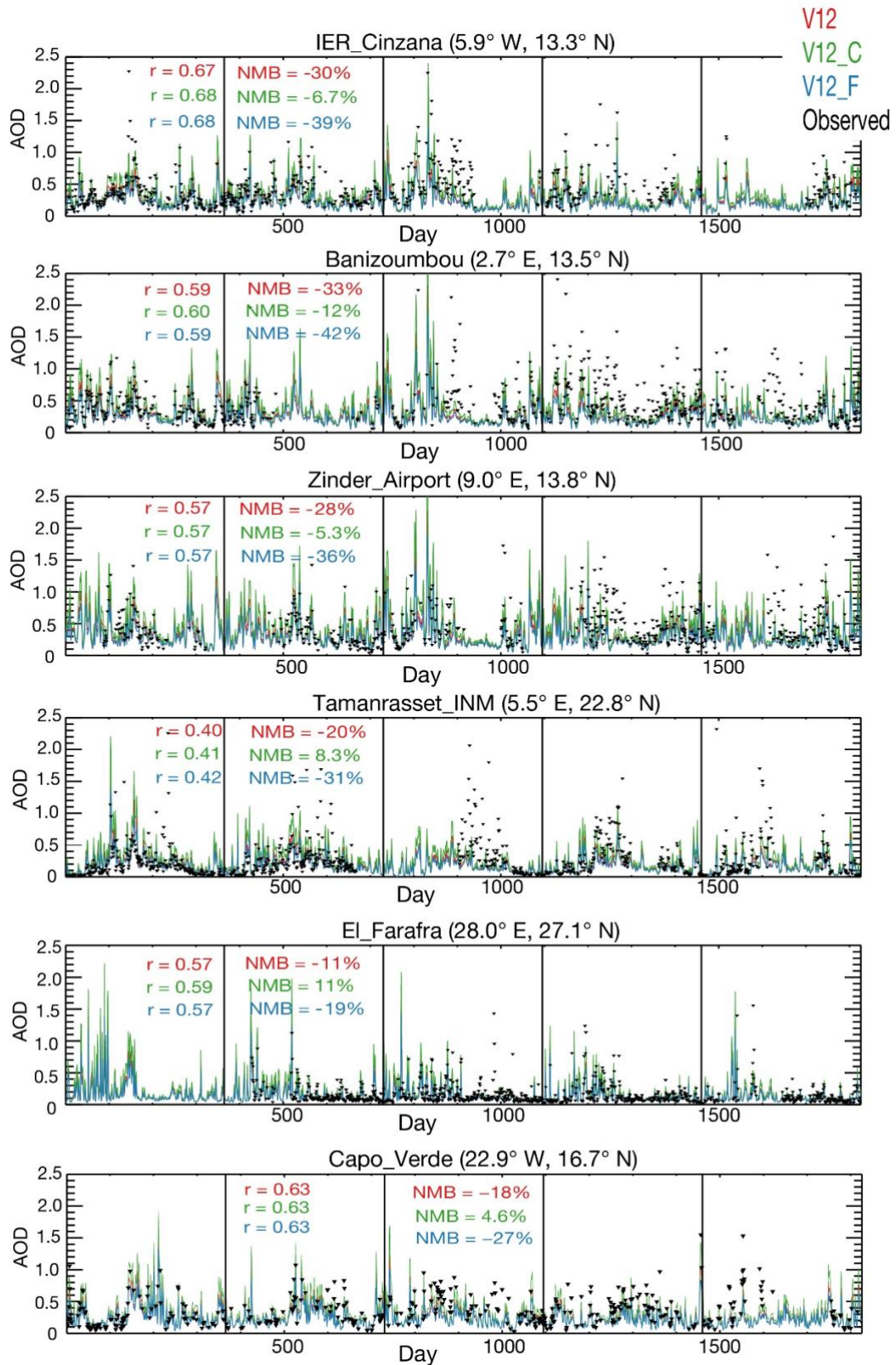
1115

1116 **Figure 3.** Time series of AERONET (black lines) and simulated daily AOD (at wavelength of 675

1117 nm) during 2013 – 2017. Normalized mean bias (NMB) and correlation (*r*) statistics between the

1118   AERONET and simulated data are shown as inset.

1119

1120
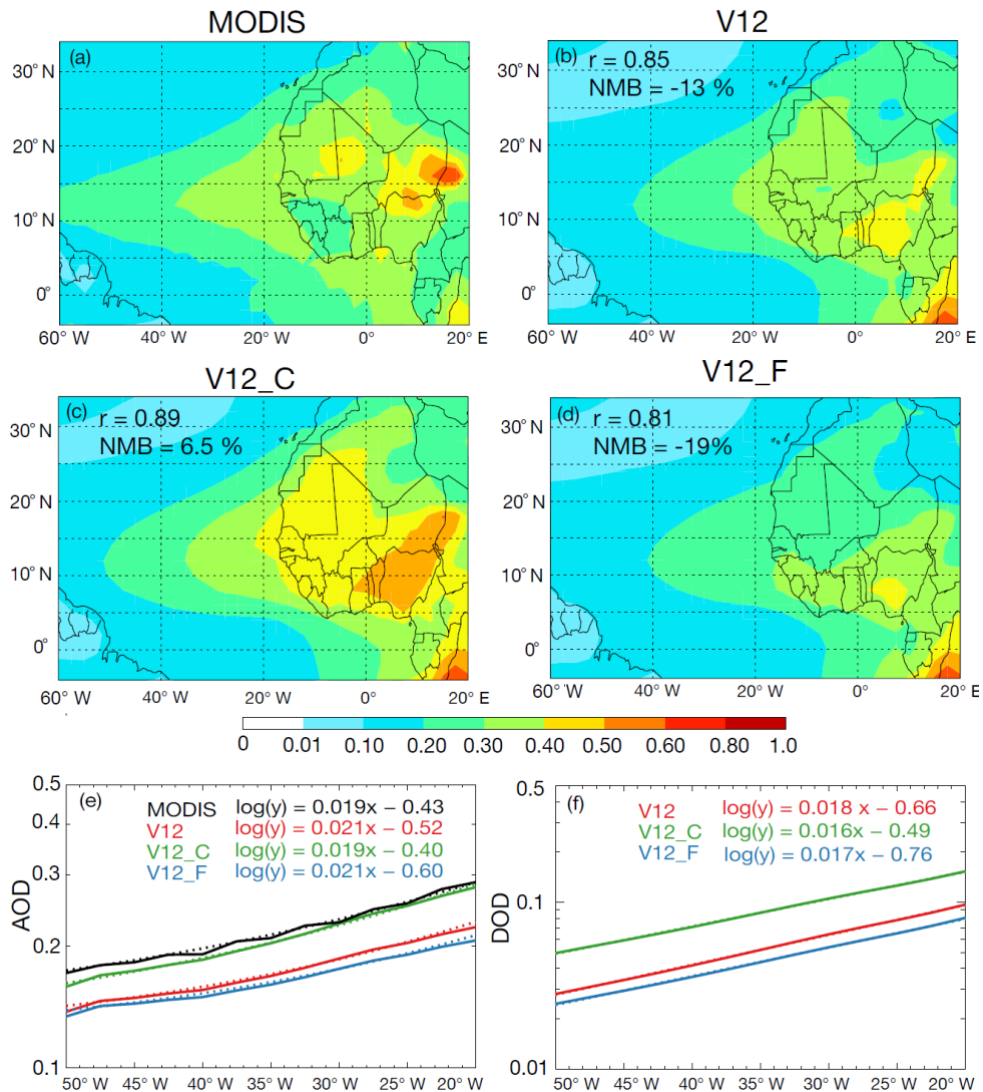
1121

1122   **Figure 4.** (a) – (d) Spatial distributions of observed and simulated AOD (at 550 nm) over the region

1123   of 60° W – 20° E and 10° N – 35° N averaged over 2013 – 2017. Normalized mean bias (NMB) and

1124   correlation coefficient (r) between the simulations and MODIS AOD are shown as inset. (e) MODIS

1125   (black) and simulated (color) AOD and (f) simulated dust optical depth (DOD) at 550 nm along the

1126   transect from 20° to 50° W, averaged over 5° S − 25° N for the period 2013 − 2017. The solid lines

1127   represent averaged data and the dashed lines are the logarithmic trend lines.

1128
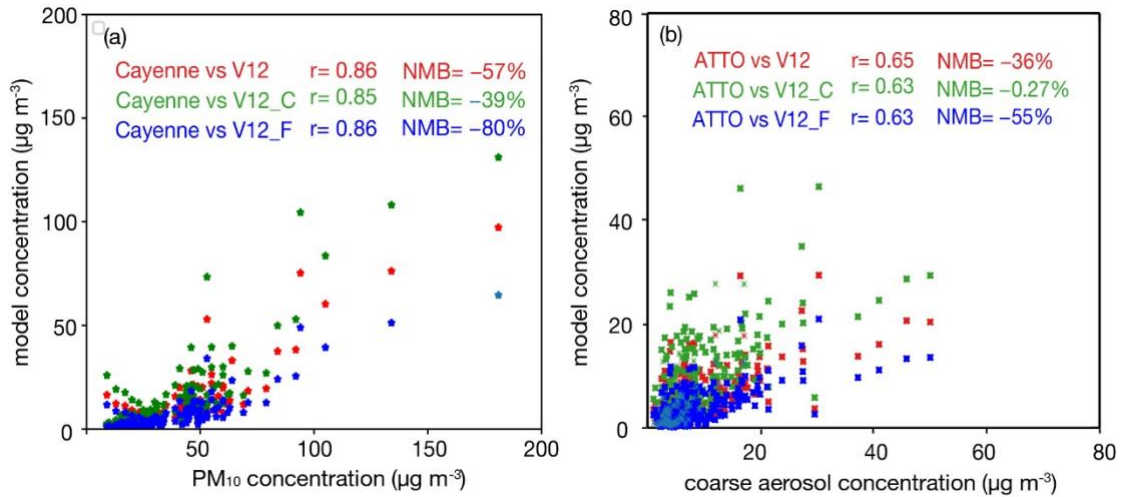
1129

Figure 5. Scatter plots of (a) observed PM_{10} and simulated dust concentrations at Cayenne site during wet season of 2014 and (b) observed coarse aerosol (PM_{1-10}) and simulated dust concentrations at ATTO site during wet season of 2014-2016. Normalized mean bias (NMB) and correlation (*r*) statistics between the observation and simulation are shown as inset.

1130
1131
1132
1133
1134
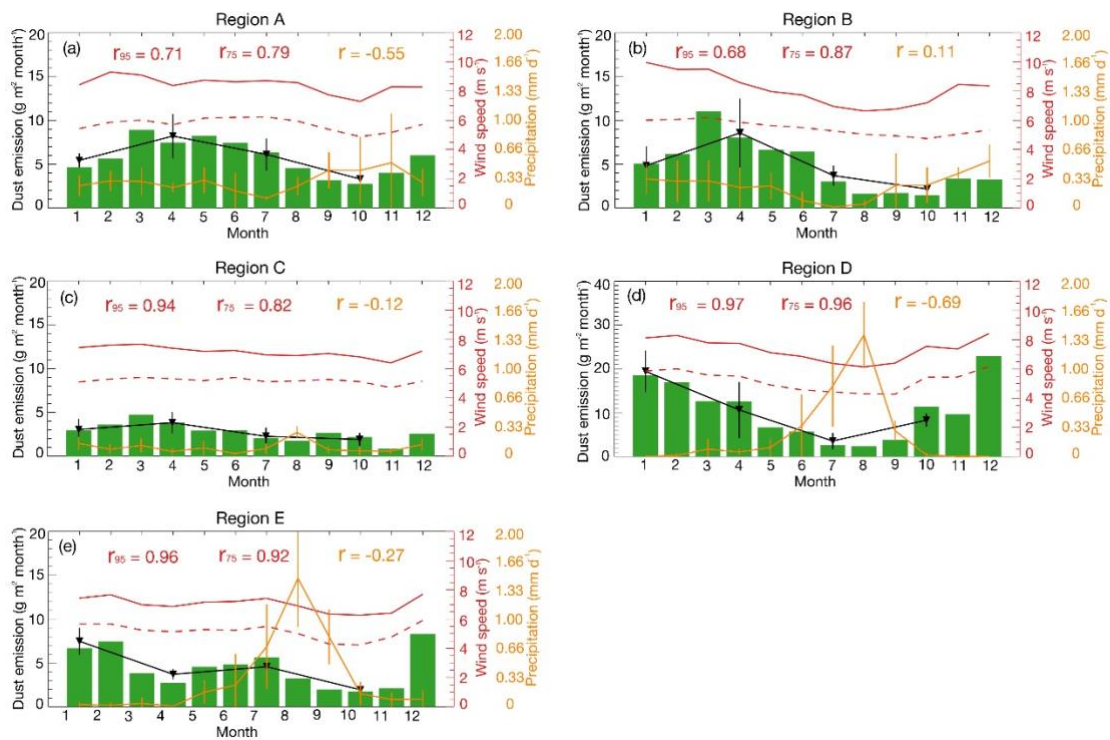
1135

Figure 6. Monthly dust emission fluxes together with the 95th percentile hourly 10-m wind speeds (red solid lines), the 75th percentile hourly 10-m wind speeds (red dotted lines) and precipitation (yellow lines) over the five major source regions averaged from 2013 to 2017. Seasonal emission fluxes of dust are also shown as black lines. The correlation coefficients (r) between the dust emission fluxes and different meteorological variables are also shown in each panel.

1136
1137
1138
1139
1140

1141

1142
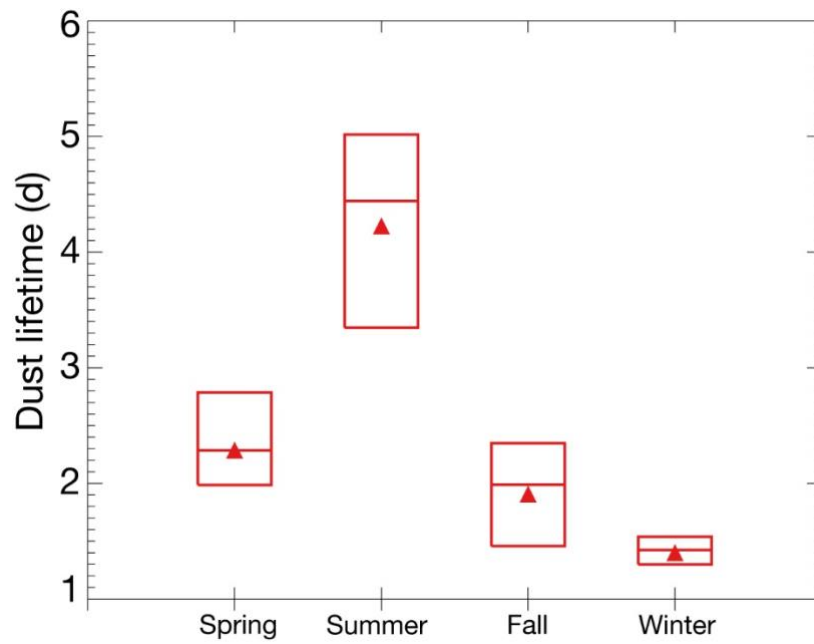
1143

1144 **Figure 7.** Seasonal e-folding lifetime derived from the logarithm of simulated dust column burden

1145 against travel time along the transect from 20° W to 50° W averaged over 5° S − 25° N during the

1146 period of 2013 – 2017. The triangles represent the mean values, and the bottom and top sides of the

1147 boxes represent the minimums and maximums.

1148
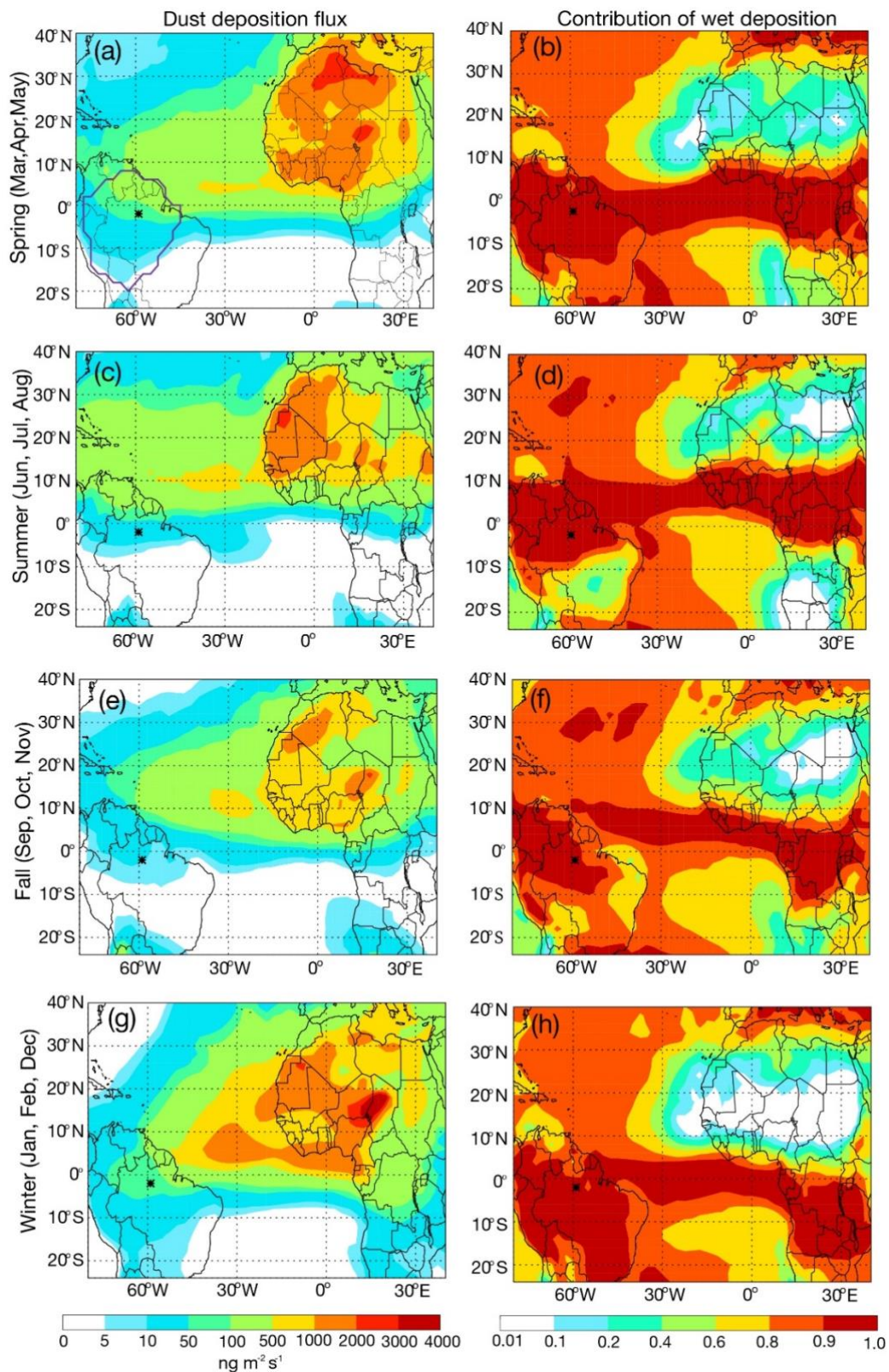
1149

Figure 8. Simulated seasonal (left) dust deposition fluxes and (right) contribution of wet deposition

during 2013-2017. The ATTO site is marked as asterisk. The region of the Amazon Basin is defined

by purple lines in Figure 8a.
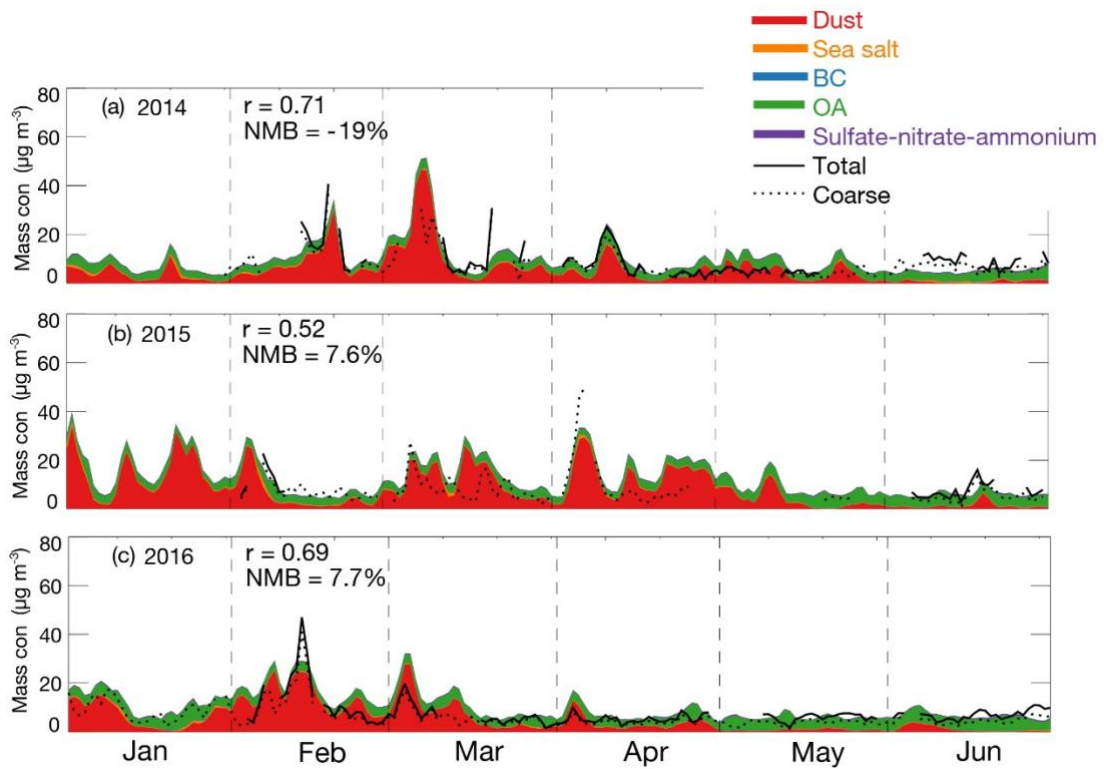
Figure 9. Time series of observed coarse and total aerosol mass concentrations and simulated aerosol species concentrations at the ATTO site from January to June in (a) 2014, (b) 2015, and (c) 2016. Model results are separated into different species shown as stacked areas. Normalized mean bias (NMB) and correlation coefficient (r) between the observed coarse aerosols and simulated dust concentrations are shown as inset.
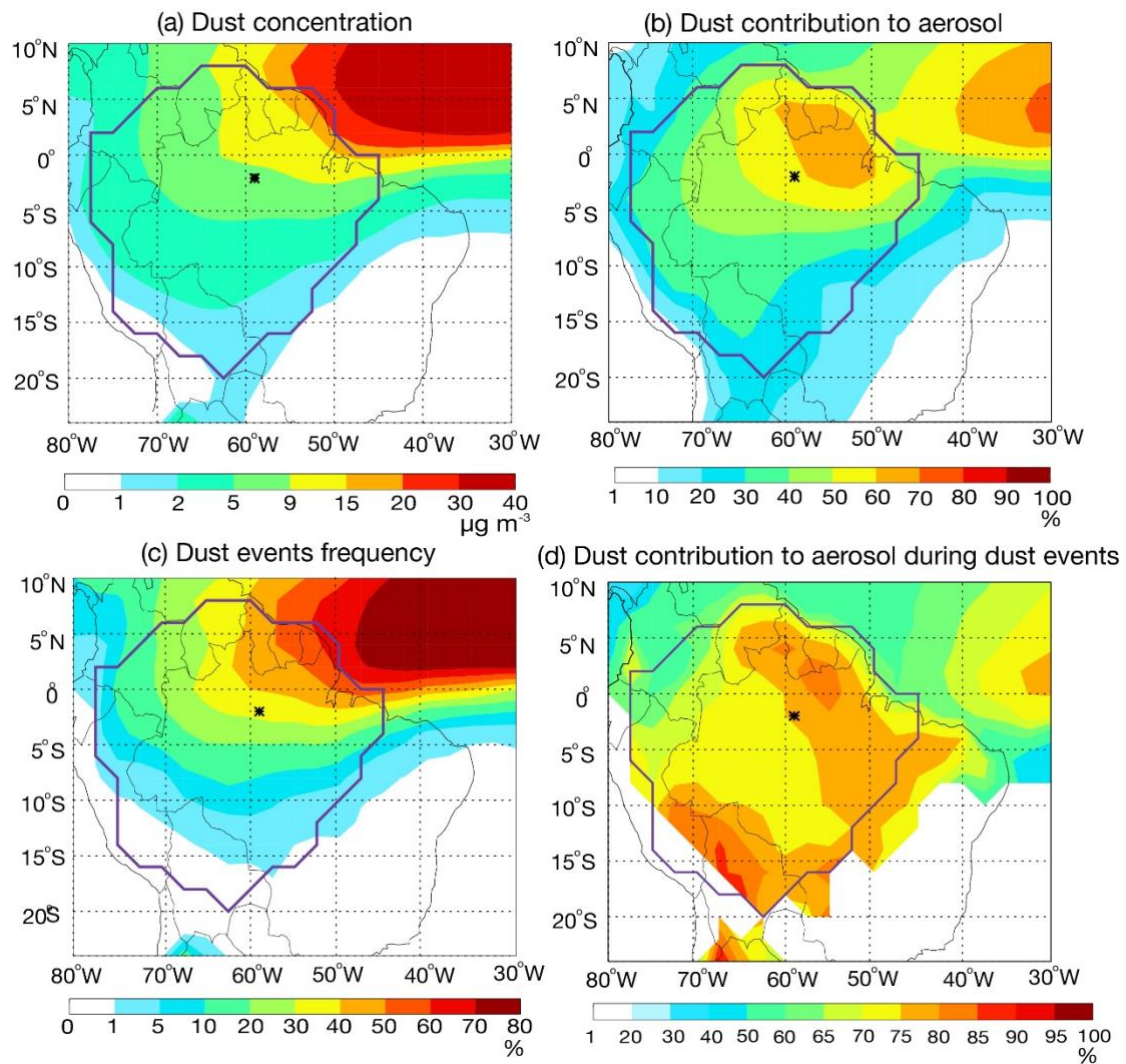
1161

1162 **Figure 10.** Dust impact over the Amazon Basin in the wet season of 2013 – 2017: (a) simulated

1163 surface dust concentrations, (b) dust contribution to surface aerosol concentrations, (c) the

1164 frequency of dust events, and (d) dust contribution to surface aerosol concentrations during dust

1165 events. The location of ATTO site is marked as asterisks. The region of Amazon Basin is marked by

1166 purple lines.

1167

1168

1169
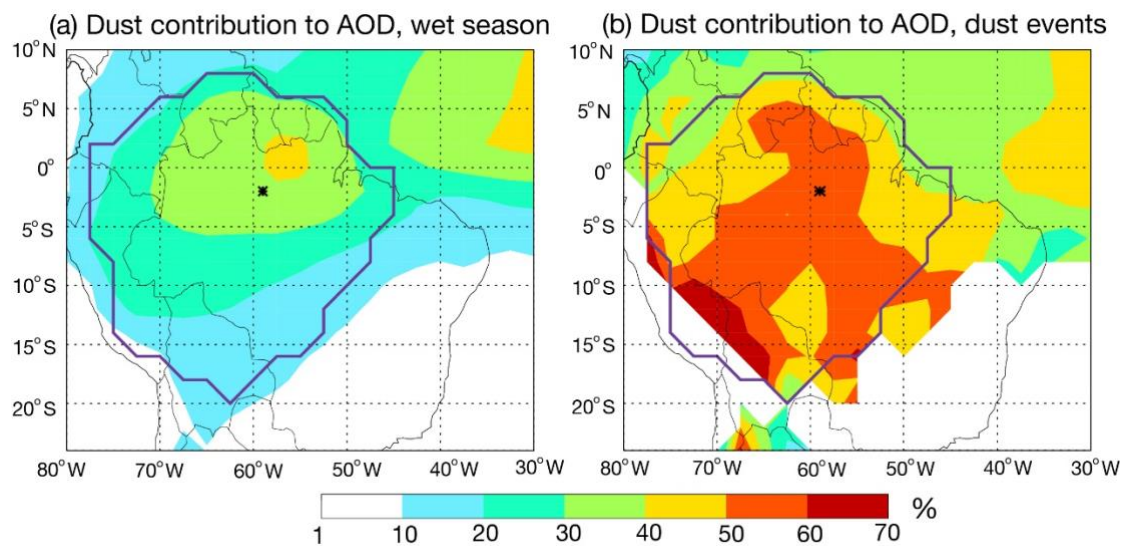
1170

Figure 11. Dust contribution to total AOD at 550 nm over the Amazon Basin averaged over the (a) wet season and (b) dust events during 2013 – 2017. The region of Amazon Basin is marked by purple lines.

1174

1175
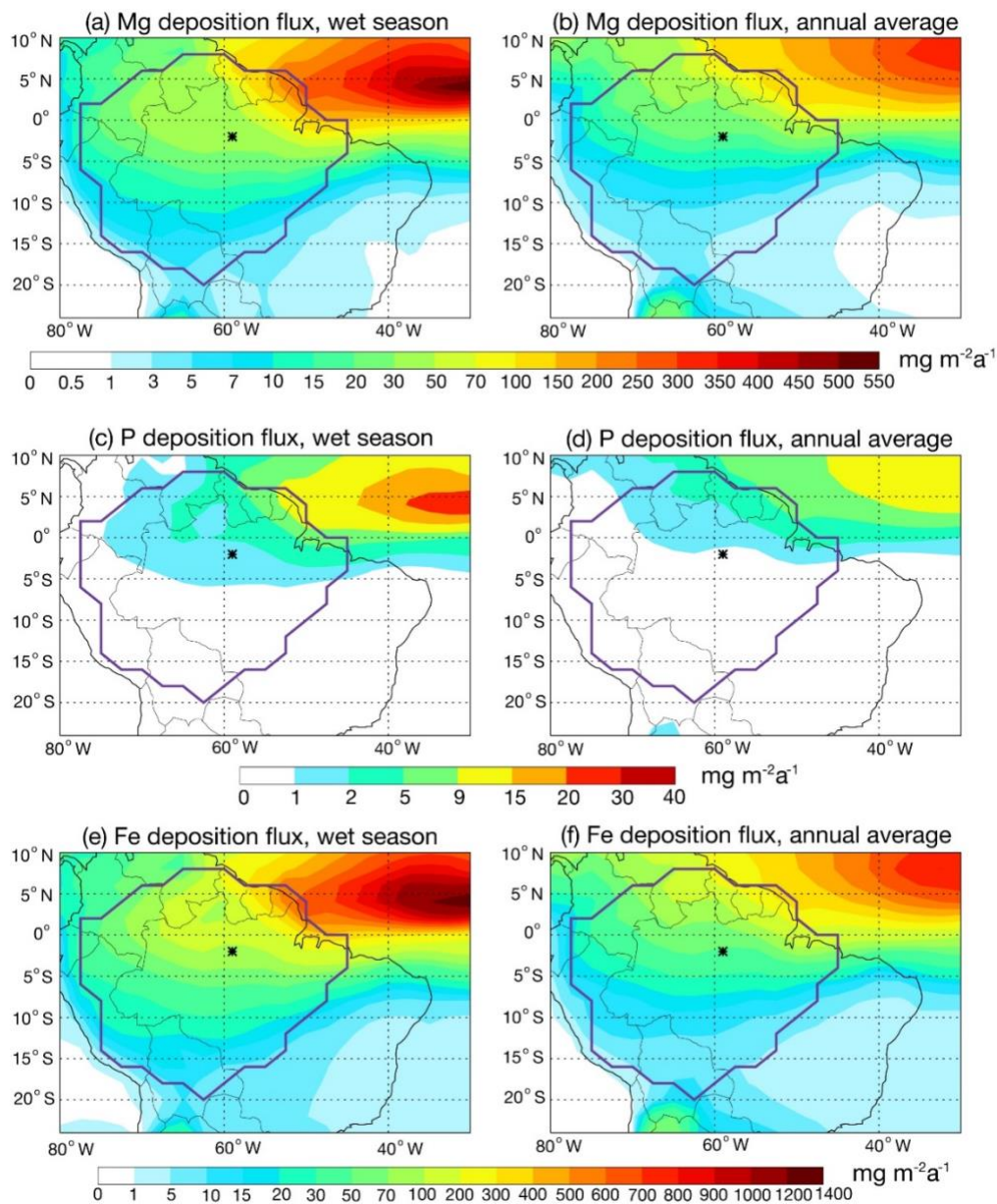
Figure 12. Magnesium deposition flux in (a) wet season and (b) annual averaged from 2013 to 2017. Phosphorus deposition flux in (c) wet season and (d) annual averaged from 2013 to 2017. Iron deposition flux in (e) wet season and (f) annual averaged from 2013 to 2017. The location of ATTO site is marked as asterisks. The region of Amazon Basin is marked by purple lines.